A Two-Source Time-Integrated Model for Estimating Surface Fluxes Using Thermal Infrared Remote Sensing

M. C. Anderson,* J. M. Norman,* G. R. Diak,† W. P. Kustas,‡ and J. R. Mecikalski†

W_e present an operational two-source (soil+vegetation) model for evaluating the surface energy balance given measurements of the time rate of change in radiometric surface temperature (T_{RAD}) during the morning hours. This model consists of a two-source surface component describing the relation between T_{RAD} and sensible heat flux, coupled with a time-integrated component connecting surface sensible heating with planetary boundary layer development. By tying together the time-dependent behavior of surface temperature and the temperature in the boundary layer with the flux of sensible heat from the surface to the atmosphere, the need for ancillary measurements of near-surface air temperature is eliminated. This is a significant benefit when T_{RAD} is acquired remotely. Air temperature can be strongly coupled to local biophysical surface conditions and, if the surface air and brightness temperature measurements used by a model are not collocated, energy flux estimates can be significantly corrupted. Furthermore, because this model uses only temporal changes in radiometric temperatures rather than absolute temperatures, time-independent biases in T_{RAD}, resulting from atmospheric effects or other sources, do not affect the estimated fluxes; only the time-varying component of corrections need be computed. The algorithm also decomposes the surface radiometric temperature into its soil and vegetation contributions; thus the angular dependence of T_{RAD} can be predicted from an observation of T_{RAD} at a single view angle. This capability is critical to an accurate interpretation of off-nadir measurements from polar orbiting and geosynchronous satellites. The performance of this model has been evaluated in comparison with data collected during two large-scale field experiments: the first International Satellite Land Surface Climatology Project field experiment, conducted in and around the Konza Prairie in Kansas, and the Monsoon '90 experiment, conducted in the semiarid rangelands of the Walnut Gulch Watershed in southern Arizona. Both comparisons yielded uncertainties comparable to those achieved by models that do require air temperature as an input and to measurement errors typical of standard micrometeorological methods for flux estimation. A strategy for applying the two-source time-integrated model on a regional or continental scale is briefly outlined. ©Elsevier Science Inc., 1997

* Department of Soil Science, University of Wisconsin-Madison, Madison

† Cooperative Institute for Meteorological Satellite Studies, Space Science and Engineering Center, University of Wisconsin-Madison, Madison

‡ USDA-ARS-Hydrology Laboratory, BARC-West, Beltsville, Maryland

Address correspondence to Dr. Martha C. Anderson, Department of Soil Science, University of Wisconsin-Madison; 1525 Observatory Drive, Madison, WI 53706.

INTRODUCTION

Thermal infrared observations of the earth's surface acquired from a satellite platform have long been recognized as a valuable key to evaluating the surface energy balance over large regions (Idso et al., 1975; Price, 1980). However, after more than 20 years of research in the remote sensing community, considerable disparity still exists in the quality of results generated by studies exploring the potential for inferring regional-scale surface fluxes from satellite data. The recent studies of Brutsaert et al. (1993) and Diak and Whipple (1995), for example, detail sensible heating estimates obtained by using satellite-measured surface temperatures that compare well with in situ measurements, whereas other in-

vestigators (Hall et al., 1992; Sellers et al., 1995; Cooper et al., 1995) have expressed a certain amount of pessimism concerning the potential value of thermal infrared remote sensing as a reliable predictor of surface energy fluxes on a regional scale.

The model developed in this paper addresses many of the stumbling blocks that have historically hindered the progress toward an operational program for monitoring surface fluxes from space. Reviews of existing models and the challenges involved in such modeling efforts are provided by Norman et al. (1995a) and Kustas and Norman (1996). A major dilemma frequently cited in the literature is that models that are general enough to predict fluxes with reasonable accuracy over a wide variety of surfaces often require a sufficiently detailed characterization of surface soil and vegetation properties and local meteorological conditions that application on regional scales has been intractable. Simpler models that parameterize many of these characteristics often require empirical tweaking from site to site, rendering them ineffectual in large-scale applications. Many models have suffered from a misuse or misinterpretation of the radiometric surface temperature (T_{RAD}) [see Norman and Becker (1995) for a discussion of the nomenclature associated with infrared thermometry]. For example, T_{RAD} is often assumed to be equivalent to the so-called aerodynamic temperature (T_{AERO}) of the surface, a bulk temperature appropriate for calculating heat transfer in the atmospheric surface layer. The interpretation of T_{RAD} is further complicated by the fact that the radiometric temperature of a surface can vary significantly, depending on the angle at which it is viewed. Biases in measured brightness temperatures, introduced by atmospheric attenuation of surface radiance when acquired at a satellite platform or by unrepresentative spatial sampling when acquired closer to the surface, can significantly degrade flux estimates, even though the absolute magnitude of this bias may be small. Finally, regional-scale flux models are difficult to validate and are therefore, on principle, subject to some degree of skepticism.

The two-source time-integrated model (hereafter, the TSTIM) presented here synthesizes important lessons learned during two decades of research in this area. It relates the morning rise in the temperature of a partially vegetated surface to the growth of the overlying planetary boundary layer through an estimate of surface sensible heating. The TSTIM is intended for application over large spatial grids and thus attempts to balance the competing demands of generality and simplicity; it has been designed to accommodate varying surface conditions while remaining computationally inexpensive and requiring only a tractable array of surface parameters.

The TSTIM is a modification of the two-source (soil+vegetation) surface model (hereafter, the TSM) of Norman et al. (1995b), which estimates instantaneous heat fluxes given single measurements of surface brightness

temperature and air temperature. Two-source models represent an advance over single-layer surface models that treat the earth's surface as a single, uniform layer (see, e.g., Hall et al., 1992; Gash, 1987; and Jackson, 1982). Single-layer models typically use T_{RAD} in place of T_{AERO} and link the sensible heat flux to the difference between T_{RAD} and the air temperature through a single aerodynamic resistance. This approach tends to overestimate sensible heat, especially over sparse canopies, because the resistance to heat transport from the soil component of the field of view is often significantly larger than the resistance above the canopy. If the difference between soil and canopy resistances is not treated explicitly by a model, the aerodynamic resistance must be increased by empirical adjustments related to the roughness length for heat transport (Kustas et al., 1989; Sugita and Brutsaert, 1990; Kohsiek et al., 1993) or by the inclusion of an empirical site-specific "additional resistance" term (Stewart et al., 1994), to obtain an agreement between measured and modeled sensible heat fluxes. The relation between T_{RAD} and T_{AERO} can be more appropriately treated if the net surface flux is apportioned among the sources from which it emanates.

Another advantage of the two-source approach is that it accommodates the view angle dependence of surface brightness temperature measurements; the variation of T_{RAD} with sensor view angle can be predicted if the individual temperatures of the soil and vegetation components in the scene can be extracted from the composite surface temperature. View angle effects are most pronounced for sparse canopies, where changes in view angle cause large differences in the fractions of vegetation and bare soil within the footprint of the radiometer. Directional variations in surface emissivity also can induce slight variations of brightness temperature with view angle (Anton and Ross, 1987; Norman et al., 1990). Surface radiometric temperatures collected by Vining and Blad (1992) at a location within the first international satellite land surface climatology project (ISLSCP) field experiment (FIFE) site show differences of as much as 5 C° when acquired at nadir and 60 degrees in zenith angle (Hall et al., 1992). The same sort of relations have been shown within a modeling context (Norman et al., 1990). Correction of observed brightness temperatures for view angle effects is of great importance when the temperatures are to be obtained from satellite images, where major portions of the image are acquired at off-nadir viewing angles.

The TSM is improved on here by the incorporation of a simple description of planetary boundary layer dynamics. This modification is inspired by the more complex combined soil-plant-atmosphere and planetary boundary layer models of Carlson et al. (1981), Wetzel et al. (1984), Taconet et al. (1986), and others; such combined models are able to simulate their own near-surface meteorological conditions and are thus less susceptible to
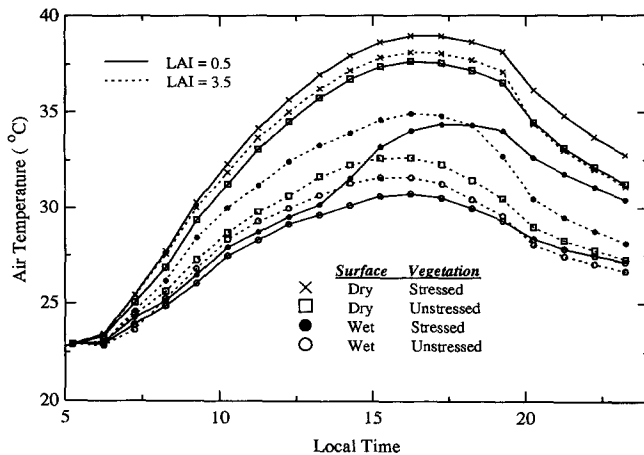
Figure 1. Variation in air temperature at 2 m above a surface with a vegetative cover 0.6 m in height, as predicted by a combined soil-plant-atmosphere and planetary boundary layer model. The words "dry" and "wet" refer to the condition of the soil surface, and the words "stressed" and "unstressed" refer to the available water (below the surface) in the root zone and thus the water status of the plant. All model runs began at 5:00 A.M. local time with the same air temperature.

errors incurred in the mismatch (both spatial and temporal) between remotely sensed and ground-based measurements. Models without a boundary layer component generally require measured air temperatures as an ancillary data input. In remote applications, where these data must be spatially (and temporally) interpolated between weather station measurements to match the thermal satellite image grid, this requirement can prove quite problematic. Air temperature can be strongly coupled to local surface characteristics that may vary appreciably over small spatial scales (e.g., vegetation cover and soil moisture), so interpolation may yield poor local estimates.

Figure 1 demonstrates the magnitude of this sensitivity. The diurnal air temperature curves in Figure 1 were generated by the Cupid soil-plant-atmosphere model (Norman and Campbell, 1983), coupled with a Mellor-Yamada second-order closure model of the planetary boundary layer (Mellor and Yamada, 1974). Leaf area index (LAI), soil surface water content, and water content in the root zone below the surface were varied independently to study the effects of surface properties on the equilibrium air temperature measured 2 m above the ground, the height of a typical weather station measurement. Figure 1 indicates that a heterogeneous surface can induce spatial variations of several degrees in near-surface air temperature. This level of variation can significantly corrupt flux estimates; for a canopy 1 m in height and a wind speed of 5 m s^{-1}, Norman et al. (1995a) predict an additional error of 40 W m^{-2} in estimated sensible heat for each degree C error in the assumed difference between surface and air temperature.

The TSTIM does not rely on measured air temperatures and thus is much better suited to large-scale applications than the TSM and other algorithms that do.

Whereas the TSM uses an instantaneous measurement of surface temperature, the TSTIM relates surface fluxes to the time rate of change in surface temperature. This practice, derived from the methods of Price (1980), Carlson et al. (1981), Wetzel et al. (1994) and other "thermal inertia moisture availability" methods for evapotranspiration estimation that exploit the correlation between the amplitude of the diurnal surface temperature wave and soil moisture content [see reviews by Carlson (1986) and Norman et al. (1995a)], renders the TSTIM insensitive to fairly large biases in measured brightness temperature. Although absolute surface radiometric temperatures derived from satellite measurements are subject to errors in sensor calibration, a general lack of information on the surface emissivity, and potential errors in atmospheric corrections, the time-independent component of these errors falls out when temporal changes are computed. Similarly, the effect of biases in surface temperature due to spatial sampling (Goetz et. al., 1995) are reduced by using time differences, as are the effects of view angle dependence (Diak and Whipple, 1995). The TSTIM uses the morning rise in surface temperature as its driving input, in accord with Wetzel et al. (1984), who find this to be the signature in the diurnal surface temperature wave most closely correlated with soil moisture content; furthermore, they note that mid-morning meteorological conditions are well suited for this type of investigation, because advection is typically at a minimal level and skies are most likely to be clear.

To the authors' knowledge, the TSTIM represents a unique combination of the aforementioned features: generality, computational simplicity, the ability to accommodate off-nadir sensor view angles, insensitivity to biases in measured brightness temperatures, and freedom from the need for ground-based air temperature measurements [see comparison with other thermal infrared models in Table 2 of Kustas and Norman (1996)]. The physical foundations for the TSTIM are developed in the next section. Because it is difficult to obtain surface flux measurements on the spatial scale of a satellite image pixel, the efficacy of the model is first validated in comparison with measurements made during the first ISLSCP field experiment (FIFE), conducted in a tall-grass prairie in Kansas (Sellers et al., 1988), and the Monsoon '90 experiment, conducted in the semiarid rangelands of Arizona (Kustas et al., 1991); future papers will explore applications to Geostationary Operational Environmental Satellite (GOES) imagery. The field experiment comparisons are discussed in the third section. The fact that the model produces good results in both vegetative regimes indicates generality—a necessity if it is to be applied on regional or continental scales. An examination of the sensitivity of the model to the input parameters that it re-

quires is provided in the fourth section, along with suggestions for acquiring these parameters on a regional basis for satellite applications. Concluding remarks are made in the fifth section.

MODEL DESCRIPTION

The two-source surface layer model of Norman et al. (1995b) forms the basic building block for the new two-source time-integrated model presented here. In this development, the TSM is coupled with a time-integrated description of planetary boundary layer growth. This results in a model that is less susceptible to systematic biases in surface temperature measurement and no longer requires measured air temperature as in input.

A brief overview of the model is provided here to guide the reader through the next section. The model is driven by two measurements of surface brightness temperature, acquired during the morning over a 4-h interval. The surface layer component of the TSTIM relates each surface temperature measurement to an estimate of instantaneous sensible heat flux by means of a computed air temperature. The time-integrated sensible heat flux during this interval is computed from these instantaneous estimates, assuming that sensible heating increases linearly with time during the morning hours. Another time-integrated flux is computed by the planetary boundary layer (PBL) component of the TSTIM; this flux is commensurate with the temporal change in air temperature derived by the surface layer component of the model and with the lapse rate structure in the overlying boundary layer. These time-integrated fluxes are compared, and through iterative cycling, the TSTIM converges on estimates for sensible heat and air temperature consistent with the measured surface temperatures.

The Two-Source Time-Integrated Model

The Two-Source Surface Layer Component
The directional radiometric temperature of a surface, $T_{RAD}(\varphi)$, can be obtained from a measurement of surface brightness temperature, $T_B(\varphi)$, acquired by satellite (after correction for atmospheric effects) or by ground-based radiometry:

$$T_B(\varphi) = \{\varepsilon(\varphi)[T_{RAD}(\varphi)]^n + [1 - \varepsilon(\varphi)](T_{SKY})^n\}^{1/n} . \quad (1)$$

Here, $\varepsilon(\varphi)$ is the directional thermal emissivity of the surface at a view zenith angle φ, T_{SKY} is the hemispherical sky brightness temperature (Norman and Becker, 1995), and n is the power in the Stefan-Boltzmann equation appropriate for the wavelength band of the sensor. Typically, $n=4$ is used for wavelength bands of 8–14 and 10–12 μm over a limited temperature range (Becker and Li, 1990).

The radiometric temperature of a vegetated surface is an ensemble average of the individual thermodynamic temperatures of the soil (T_s) and vegetation (T_c) lying within the sensor field of view, weighted by their contribution to the brightness temperature:

$$T_{RAD}(\varphi) = \{f(\varphi)T_c^n + [1 - f(\varphi)]T_s^n\}^{1/n} , \quad (2)$$

where $f(\varphi)$ is the fraction of the sensor field of view occupied by vegetation when viewed at a zenith angle φ. The temperatures T_c and T_s are themselves spatially weighted averages over the sunlit and shaded parts of the canopy and soil, respectively. Equation (2) assumes that a single emissivity [assumed to be 0.99 at nadir; Palluconi et al. (1990)] may be attributed to each component in the scene; although soil and vegetation may exhibit different emissivities when studied individually, multiple reflections between soil and leaves tend to equalize the component emissivities in a soil-canopy system. The angular variation of directional emissivity, $\varepsilon(\varphi)$, usually results in a brightness temperature variation of less than 0.5 C° between view angles of nadir and 60° (Anton and Ross, 1987) and is neglected here.

The form for $T_{RAD}(\varphi)$ in Eq. (2) explicitly accommodates the effect of sensor view angle (φ) on observed radiometric temperature; as the soil layer becomes increasingly obscured by vegetation with increasing view zenith angle, the contribution of the soil temperature to the composite surface temperature is decreased accordingly through the weighting function $f(\varphi)$. An accurate interpretation of a surface temperature, particularly an off-nadir observation, therefore requires knowledge or estimates of $f(\varphi)$, T_c, and T_s. For ease of computation, Eq. (2) can be linearized with little loss of accuracy (<0.5 C°):

$$T_{RAD}(\varphi) \approx f(\varphi)T_c + [1 - f(\varphi)]T_s . \quad (3)$$

[For the purist, a linear adjustment can be made to Eq. (3) to improve the agreement with Eq. (2); Norman et al. (1995b).] For a canopy with a random distribution of leaves, a spherical distribution of leaf angles, and a leaf area index F,

$$f(\varphi) = 1 - \exp\left(\frac{-0.5F}{\cos\varphi}\right) . \quad (4)$$

If LAI is not known, it can be estimated from a measurement of fractional vegetation cover (Norman et al. 1995b).

In the TSM and the TSTIM, Eq. (3) is a key member of the system of equations used to estimate the partitioning of the soil and canopy energy budgets. The net balance of energy at the earth's surface, neglecting photosynthesis, can be represented by

$$R_n = H + LE + G , \quad (5)$$

where R_n is the net radiation incident above the canopy, and H, LE, and G are the net fluxes of sensible, latent, and soil conduction heating, respectively. Representing the soil and canopy components of these net fluxes with

the subscripts "s" and "c", respectively, the set of equations constituting the surface component of the TSTIM are:

Surface radiometric temperature [Eq. (3)]:

$$T_{RAD}=f(\varphi)T_c+[1-f(\varphi)]T_s \qquad (6a)$$

Soil and canopy energy budgets:

$$R_{n,s}=H_s+LE_s+G \qquad (6b)$$

$$R_{n,c}=H_c+LE_c \qquad (6c)$$

Net radiation:

$$R_n=R_{n,s}+R_{n,c} \qquad (6d)$$

$$R_{n,s}=R_n\exp(-\kappa F/\sqrt{2\cos\varphi}) \qquad (6e)$$

Sensible heat:

$$H=H_s+H_c \qquad (6f)$$

$$H_s=\rho c_p\frac{T_s-T_a}{R_a+R_s} \qquad (6g)$$

$$H_c=\rho c_p\frac{T_c-T_a}{R_a} \qquad (6h)$$

Latent heat:

$$LE=LE_s+LE_c \qquad (6i)$$

$$LE_c=a_{PT}f_g\frac{S}{S+\gamma}R_{n,c} \qquad (6j)$$

Ground conduction heat:

$$G=a_gR_{n,s} \qquad (6k)$$

In Eq. (6), $R_{n,c}$ is the net radiation absorbed by the canopy, and $R_{n,s}$ is the net radiation penetrating to the soil surface. The simple extinction law $R_{n,s}=R_n\exp(-\kappa F)$ used by Norman et. al (1995b) in the TSM assumes that the extinction of net radiation is independent of the path length through the canopy. Here we implement a more realistic form, developed through numerical experimentation with the soil-plant-atmosphere model Cupid. Equation (6e) allows the effective extinction to vary with solar angle and thus more faithfully captures the time behavior of $R_{n,s}$. We use the extinction coefficient $\kappa=0.45$, lying midway between the limits of 0.3 to 0.6 expected for most vegetation (Ross, 1981).

In accord with Choudhury et al. (1987), the flux of heat conducted into the soil (G) is parameterized as a constant function, a_g, of the net radiation at the soil surface [Eq.(6k)]. With the assumption of a time-independent extinction law for net radiation, values of a_g between 0.2 and 0.5 were obtained from measurements of above-canopy net radiation and soil heat flux at midday (Choudhury et al., 1987). Norman et al. (1995b) chose to use $a_g=0.35$ in the TSM, the midpoint of this range. A smaller fraction $(a_g=0.31)$ must be used in conjunction with the time-dependent extinction law in Eq. (6e), which yields somewhat higher transmission at midday.

Equations (6f)–(6h) assume that the fluxes of sensible heat from the soil (H_s) and vegetation (H_c) within the field of view are in parallel. Norman et al. (1995b) show that this is a reasonable assumption for sparsely vegetated surfaces; the more complicated series/parallel resistance arrangement that they describe could be used instead, but solutions would differ significantly only for dense vegetation. The quantity R_a in Eqs. (6g) and (6h) is the aerodynamic resistance to heat transport across the layer between the nominal heat exchange surface within the canopy and the height, z_T, at which the air temperature, T_a, is measured. Heat transported between the soil and height z_T must pass through the boundary layer immediately above the soil surface and thus encounters an additional resistance R_s [Eq. (6g)].

The aerodynamic resistance can be expressed as (Brutsaert, 1982)

$$R_a=\frac{\left[\ln\left(\frac{z_T-d}{z_m}\right)-\Psi_h\right]\left[\ln\left(\frac{z_U-d}{z_m}\right)-\Psi_m\right]}{k^2u}+R_{ex} . \qquad (7)$$

Here, u is the wind speed measured at height z_U; z_T is height of the air temperature measurement; k is the von Karman constant (taken to be 0.4); Ψ_h and Ψ_m are the stability corrections for heat and momentum transport, respectively; d is the displacement height; and z_m is the roughness length for momentum transport. For vegetated surfaces with canopy height h_c, $d\approx0.65h_c$ and $z_m\approx h_c/8$ (Shaw and Pereira, 1982) can be used if no direct measurements are available. The second term in Eq. (7) is often called the "excess aerodynamic resistance," because it describes the difference in resistance encountered in the transfer of scalar quantities and momentum. The term R_{ex} should not be confused with the empirical "additional resistance" term used in many single-layer models to compensate for the fact that radiometric surface temperature is being used in place of the aerodynamic temperature to compute sensible heat. In this study, we use a form for R_{ex} given by McNaughton and van den Hurk (1995):

$$R_{ex}=130\frac{\sqrt{su_*}}{F}-1.7 , \qquad (8)$$

where s is a typical leaf dimension, and $u_*=uk/\ln[z_u-d)/z_m]$ is the friction velocity. An empirical expression for R_s as a function of the parameters u, d, z_m, F, h_c, and s has been developed by Sauer et al. (1995) and is summarized by Norman et al. (1995b). This empirical model has worked well for both subhumid grasslands at the FIFE site and for a semiarid rangeland at the Monsoon '90 site containing sparsely vegetated shrub and grasslands (Norman et al, 1995b).

In the TSTIM, a first-pass estimate of the canopy transpiration rate, LE_c [Eq. (6j)], is provided by application of the Priestley-Taylor approximation (Priestley and

Taylor, 1972) to the green component of the vegetation. In this equation, a_{PT} is the Priestley-Taylor constant ($a_{PT}=1.3$), f_g is the fraction of green vegetation in the canopy, S is the slope of the saturation vapor pressure versus temperature curve, and γ is the psychrometer constant (0.066 kPa $°C^{-1}$). This approximation assumes that the canopy is transpiring at its maximum potential rate, an assumption that is often valid in regions where there is adequate water supply but tends to overestimate canopy transpiration in more arid ecosystems. Fortunately, the TSTIM provides a means of identifying situations where Eq. (6j) is invalid. If the Priestley-Taylor approximation attributes too great a portion of the net latent heat flux to the canopy, the solution of Eqs. (6a)–(6k) will cause the soil evaporation flux, LE_s, to become negative in compensation. Because condensation onto the soil is unlikely to occur under daytime conditions, the TSTIM decides in these cases that the canopy transpiration rate is water limited, and LE_c is throttled back until LE_s reaches zero [see Norman et al. (1995b) for further discussion on how this is accomplished in practice]. Norman et al. (1996) describe an alternative to Eq. (6j) involving the light-use-efficiency of carbon assimilation; this method yields a more accurate estimate of canopy transpiration but requires an additional ancillary measurement of near-surface vapor pressure. Both methods yield similar predictions for the *net* fluxes of sensible and latent heating; the characterization of LE_c mainly affects the partitioning of net fluxes between the soil and canopy.

Given measurements and/or estimates of T_{RAD}, solar radiation, surface albedo, wind speed, roughness length, and canopy height and cover; Eqs. (6a)–(6k) constitute 11 equations in 12 unknowns: T_a, T_s, T_c, $R_{n,s}$, $R_{n,c}$, H, H_s, H_c, LE, LE_s, LE_c, and G. The next section describes how a simple boundary layer model provides the information required to solve this system of equations.

The Time-Integrated PBL Development Component
The TSM operates on single, instantaneous measurements of surface brightness temperature. Geostationary satellites (such as GOES) are capable of recording the time evolution of surface temperature; these time changes contain valuable information concerning the surface soil water status (Jackson, 1982). The TSTIM takes advantage of this temporal information, using it to eliminate the need for actual ground measurements of air temperature. The temperature of the air above the earth's surface will evolve such that the energy budgets at the surface and in the planetary boundary layer are independently balanced. In this section, a simple equation describing energy conservation in the PBL is developed, which can be solved simultaneously with the surface equations [Eqs. (6a)–(6k)] for the common boundary condition of air temperature. Although more rigorous formulations for PBL development could be incorpo-
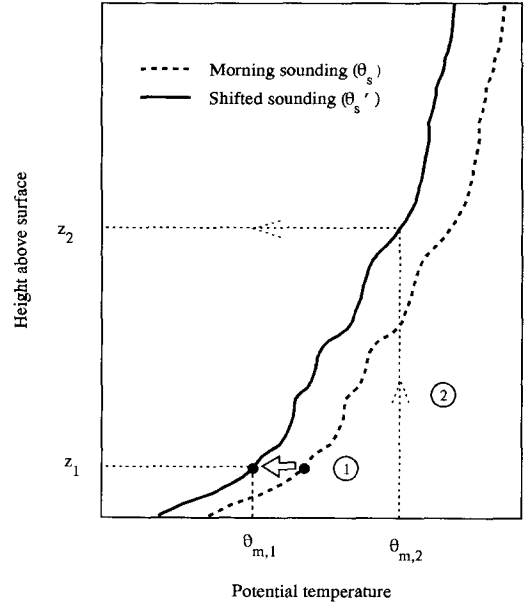

Figure 2. Schematic describing the simple procedure used in practice to diagnose boundary layer growth during the time interval from t_1 to t_2. (1) First, the initial boundary layer height is fixed at a prescribed height z_1 by shifting the early morning sounding, θ_s, in temperature until $\theta_s(z_1)$ is equal to $\theta_{m,1}$. (2) Next, z_2 is located as the intersection between an adiabat at the potential temperature of the mixed layer at time t_2 ($\theta_{m,2}$) and the shifted sounding. This method ties growth in the boundary layer to the time-change in air temperature during this interval, rather than to absolute temperature values.

rated here, the final goal for application on regional scales leads us to choose a formulation that is computationally undemanding.

The subscript "i" is used hereafter to indicate a measured or estimated quantity corresponding to a specific time t_i.

We adopt a simple slab model of the mixed layer, assuming all air within the layer to be at a uniform potential temperature, θ_m. Near the land surface (at the height at which air temperature is measured, z_T), the mixed layer potential temperature and the air temperature are related by

$$\theta_m = T_a \left(\frac{100}{p}\right)^{R/c_p}, \qquad (9)$$

where p is the atmospheric pressure (in kPa) at z_T and $R/c_p=0.286$. Further, we assume that the height of the boundary layer at a time t_i can be approximated by the height z_i at which an adiabat at the current mixed layer potential temperature, $\theta_{m,i}$, intersects an early morning temperature sounding (see the schematic in Fig. 2). A similar procedure for determining boundary layer height has been used by Tennekes (1973). Under this assump-

tion, the height of the boundary layer at all times during the convective phase is uniquely defined by the current surface air temperature [through Eq. (9)] and the morning sounding.

McNaughton and Spriggs (1986) give a simplified conservation equation describing the growth of a convective boundary layer over time, neglecting the effects of subsidence and horizontal advection:

$$\rho c_p (z_2 \theta_{m,2} - z_1 \theta_{m,1}) = \int_{t_1}^{t_2} H(t) dt + \rho c_p \int_{z_1}^{z_2} \theta_s(z) dz \quad . \quad (10)$$

Again, $\theta_{m,i}$ is the potential temperature within the mixed layer, whereas $\theta_S(z)$ is the potential temperature profile above the mixed layer at time t_1, obtained, for example, from an early morning temperature sounding. During the time interval from t_1 to t_2, the top of the mixed layer rises from height z_1 to z_2. The net growth is determined by the amount of energy supplied to the mixed layer during this time interval in the form of sensible heat and by the resistance to boundary layer growth, determined by the potential temperature profile above the initial height of the PBL, z_1.

The simple method for diagnosing boundary layer height described above may be subject to error under certain circumstances; however, the effect of such misdiagnoses on TSTIM flux estimates is expected to be small. An elevated near-adiabatic layer in the morning sounding, located above the initial PBL height, could simulate a tremendous growth rate with this method. Fortunately, the resistance to growth in this case would be small, and the error in the estimate of sensible heating required to fuel this growth is likewise small. Strong advection occurring between times t_1 and t_2 will also corrupt PBL height and sensible heat estimates if not properly accounted for. However, advection and other large-scale atmospheric effects are least significant during times in which the TSTIM is constrained to operate: during the morning and under clear-sky conditions. (Wetzel et al., 1984). Eq. (10) could be rewritten to explicitly include the effects of horizontal advection (Swiatek, 1992; Hipps et al., 1994). Although the specific cases examined in this paper were not greatly affected by including advection effects in the TSTIM, such a modification may be appropriate for more general studies.

To relate the time-integrated sensible heating in Eq. (10) to the instantaneous flux estimates provided by the surface layer component of the TSTIM [Eq. (6f)], a simple functional form for $H(t)$ is assumed. In the morning hours, from shortly after sunrise until just before local noon, sensible heating increases approximately linearly with time. On the basis of the studies of Deardorff (1967), Tennekes (1973) suggests the form

$$H(t) = \frac{H_N}{T} t \quad , \quad (11)$$

where H_N is a scaling flux, and T is a flux rise time (Tennekes suggests 3 h). An examination of the diurnal cycle

of sensible heat measurements from the FIFE and Monsoon '90 experiments indicates that t is best referenced to 1 h after sunrise. Combining the integral of Eq. (11) with Eq. (10) and substituting $H_i \, T/t_i$ for H_N [Eq. (11)] yields the following expression for the sensible heat flux at time t_i during this linear phase:

$$H_i = \frac{2\rho c_p t_i}{(t_2^2 - t_1^2)} [z_2 \theta_{m,2} - z_1 \theta_{m,1} - \int_{z_1}^{z_2} \theta_s(z) dz] \quad . \quad (12)$$

Equation 12 assumes that the temperatures in the sounding, $\theta_s(z)$, are consistent with the air temperature estimates generated by the surface-layer component of the model. In many applications, however, local atmospheric soundings will be unavailable—the nearest radiosonde station may be hundreds of kilometers away from the site of the surface temperature measurement. Furthermore, any systematic bias in the measured surface temperatures will translate into a bias in the estimates of θ_{mi}, effectively shifting the limits of integration in Eq. (12). Because the time-change in surface temperature is more reliable than are absolute temperature measurements, in practice we fix the height of the boundary layer at the first observation time (z_1), and allow the *change* in modeled θ_m to govern the growth of the boundary layer. We assume that the height of the boundary layer early in the morning is some small fixed value $(z_1 \approx 50 \text{ m})$ and shift the sounding in temperature such that $\theta_s(z_1)$ is equal to $\theta_{m,1}$, (see Fig. 2). The integral in Eq. (12) is performed over this shifted sounding, $\theta_s'(z_1)$.

Solving the TSTIM Surface and PBL Energy Budget Equations

The joint solution to the surface and PBL energy budget equations in the TSTIM can be summarized as follows. Combining Eqs. (9) and (12) from the PBL component of the TSTIM yields

$$H_i = \frac{2\rho c_p t_i}{t_2^2 - t_1^2} \left[\left(\frac{100}{p} \right)^{R/c_p} (z_2 T_{a,2} - z_1 T_{a,1}) - \int_{z_1}^{z_2} \theta_s(z) dz \right] \quad . \quad (13)$$

Combining Eqs. (6f)–(6h) and (6a) from the surface component yields

$$T_{RAD,i} = T_{a,i} + f(\varphi) \frac{H_{c,i} R_{a,i}}{\rho c_p} + [1 - f(\varphi)] \quad (14)$$

$$\times \frac{(H_i - H_{c,i})(R_{a,i} + R_{s,i})}{\rho c_p} \quad ,$$

where a first-pass estimate of $H_{c,i}$ is obtained from Eqs. (6c) and (6j):

$$H_{c,i} = R_{n,c,i} \left[1 - a_{Pr} f_g \frac{S}{S+g} \right] \quad . \quad (15)$$

(Again, this estimate can be amended if it fails to produce realistic predictions for the soil evaporation rate). Equations (13)–(15) are applied twice during the morning hours, at time t_1 and t_2 (the optimal choice for these sampling times is discussed in the next section). Because
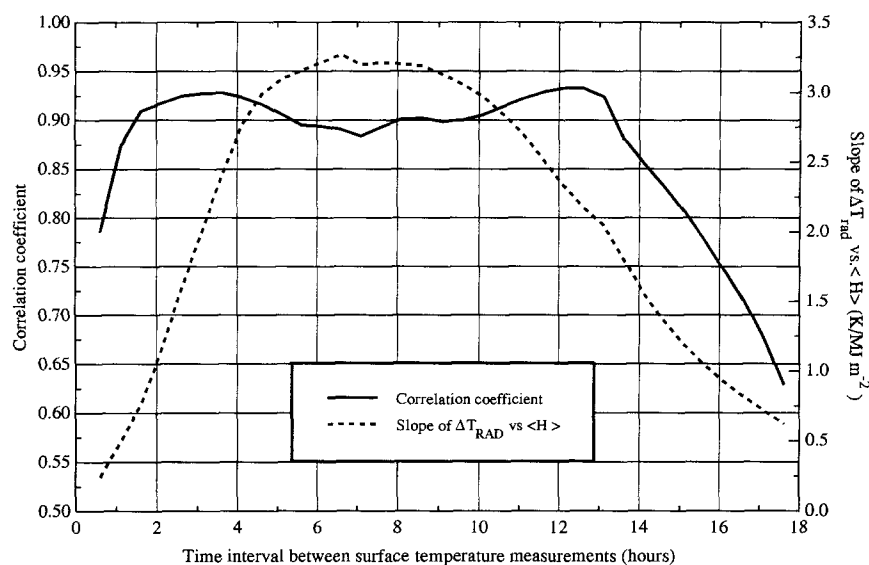
Figure 3. The correlation between morning rise in surface temperature (ΔT_{RAD}) and daytime total sensible heat flux ($\langle H \rangle$) vs the time interval between T_{RAD} measurements, assuming that the first measurement is made 1.5 h after sunrise. Also plotted is the slope of ΔT_{RAD} vs $\langle H \rangle$ as a function of time interval. These results are based on a combined soil-plant-atmosphere (Cupid) and PBL model.

z_1 and z_2 are determined by $T_{a,1}$ and $T_{a,2}$ under our assumptions and $\theta_s(z)$ is given by the early morning sounding, the unknowns in these equations are H_1, H_2, $H_{c,1}$, $H_{c,2}$, $T_{a,1}$, and $T_{a,2}$. Thus, given measurements of radiometric surface temperature at times t_1 and t_2, Eqs. (13)–(15) yield six equations that can be solved for the six unknowns. The remaining component and composite fluxes and temperatures at times t_1 and t_2 can be obtained from the Eq. (6a)–(6k). This solution can be easily extended to additional times during the morning if the commensurate brightness temperature measurements are available.

The ancillary data requirements for the TSTIM are similar to those for the TSM, with one important exception. In situ air temperature measurements are not needed—they are computed by the TSTIM. In lieu of measured air temperatures, the TSTIM requires a description of PBL lapse rate structure in the early morning. Sensitivity tests suggest that the TSTIM is not significantly affected by relatively large errors in lapse rate specification (see the section on parameter sensitivity).

Selection of an Optimal Time Pair

Experimentation with the TSTIM has shown that the choice of limits in the time-integral in Eq. (10) can affect the accuracy of the estimated surface fluxes. Obviously, times must be chosen such that the assumption of a linear rise in sensible heat [Eq. (11)] applies. This limits the choice of the upper limit to times at least an hour before local noon. Immediately after sunrise, the surface sensible heat flux is channeled into dissipating the shallow surface inversion that has developed overnight, and the PBL energy conservation equation [Eq. (10)] does not hold. The first observation of surface temperature should therefore occur at least an hour after sunrise. Within these constraints, the observations of surface temperature should be spaced far enough in time so that a strong temperature change signal is detected.

The Cupid surface layer model (Norman and Campbell, 1983), coupled with a one-dimensional, second-order closure PBL model (Mellor and Yamada, 1974), was used to identify a pair of observation times that would prove optimal over a variety of surface condition scenarios. Surface and PBL data collected during the FIFE experiment on 7 July 1987 were used to drive multiple model runs representing varying conditions in LAI, soil moisture content and wind speed. These simulations show that, for a given wind speed, the daytime average sensible heat flux is well correlated with the temporal change in surface radiometric temperature and that the degree of correlation depends on the choice of time interval over which temperature change is computed. This dependence is illustrated in Figure 3, assuming that the first measurement is obtained 1.5 h after sunrise. Also plotted here is the *slope* of the relation between temperature change and daytime averaged sensible heat for different choices of time interval; with higher slopes, small differences in sensible heating will be distinguished by larger signals in surface temperature change. The best choice of time interval will be that which maximizes both of these curves while satisfying the aforementioned constraints.

On these bases, we have chosen in this investigation to use radiometric surface temperature measurements acquired at 1.5 and 5.5 hours past sunrise, yielding a time interval between measurements of $t_2-t_1=4$h. Note that, though this choice appears appropriate for early July, the selection of an optimal time pair may very well be seasonally dependent owing to variations in the relative rate of heating as day length and solar angle change.

Extrapolating to a Total Daytime Flux

For many purposes, a surface flux integrated over the daylight hours is of more use than an instantaneous flux estimate. One way to extrapolate from an instantaneous

flux estimate to a daytime total is to assume that the surface energy budget is "self-preserving"; that is, that the relative partitioning among components of the budget remains constant throughout the day. For example, Hall et al. (1992) use FIFE data to show that the "evaporative fraction," given by the ratio between latent heat and the available energy flux

$$f_{\text{evap}} = \frac{LE}{R_n - G} \; , \tag{16}$$

is stable during the daytime hours. In a similar study conducted in Arizona (Jackson et al., 1983), instantaneous fluxes were scaled to daily fluxes with good success by using solar radiation in place of the available energy flux in Eq. (16). An estimate of the daytime total $\langle R_n \rangle - \langle G \rangle$ can be computed from a time series of net radiation measurements [see Eqs. (6e) and (6k)]. The remaining daily budget components can then be estimated with

$$\langle LE \rangle = f_{\text{evap}}(\langle R_n \rangle - \langle G \rangle) \; , \tag{17}$$

$$\langle H \rangle = \langle R_n \rangle - \langle G \rangle - \langle LE \rangle \; . $$

An examination of surface flux data from the FIFE experiment and the Monsoon '90 experiment showed that the evaporative fraction computed from fluxes measured at 5.5 h past sunrise (time t_2) tends to underestimate the daytime average by about 10%; f_{evap} continues to increase slightly into the afternoon. Other studies have also shown that the self-preservation method yields daytime latent heat estimates that are smaller than observed values by 5–10% (Gurney and Hsu, 1990; Sugita and Brutsaert, 1991; Brutsaert and Sugita 1992). Therefore, in extrapolating from instantaneous to daytime surface fluxes, we have used an evaporative fraction given by

$$f_{\text{evap}} = 1.1 \frac{LE_2}{R_{n,2} - G_2} \; , \tag{18}$$

where $R_{n,2}$ is the observed net radiation at time t_2, and LE_2 and G_2 are the latent and soil heat fluxes estimated by the TSTIM at t_2.

MODEL VALIDATION

The surface flux databases used by Norman et al. (1995b) to evaluate the performance of the TSM are used here in assessing the TSTIM. The first ISLSCP field experiment was conducted in a 15×15 km region near Manhattan, Kansas, in 1987 and 1989 in and around the Konza Prairie Research Natural Area. The vegetation cover at this site is variable over small spatial scales, with LAI varying from less than 0.5 to approximately 3. A comprehensive description of FIFE can be found in Sellers et al. (1988) and Sellers et al. (1992). The Monsoon '90 experiment was conducted in 1990 near Tombstone, Arizona, in the Walnut Gulch Experimental Watershed

maintained by the USDA-ARS Southwest Watershed Research Center. Walnut Gulch is a semiarid rangeland, more sparsely vegetated than the FIFE site. Details concerning this experiment are provided by Kustas et al. (1991) and Kustas and Goodrich (1994). Single-layer models have typically had difficulty accommodating both sparse and well-vegetated surfaces without resorting to empirical adjustments (Kustas et al., 1989; Stewart et al., 1989). These databases, therefore, provide a good test of the generality of the TSTIM.

In field experiments such as the FIFE and Monsoon '90, the surface can be characterized in much greater detail than is practical on the scale of a satellite image. Furthermore, the scaling of many surface parameters from meter to kilometer spatial scales is not straightforward (Price, 1990). Nevertheless, validation with micrometeorological measurements is an important first step in constructing a flux model destined to perform on larger scales. Many algorithms that have been proposed for satellite image analyses have never been tested against actual measurements, and thus their effectiveness can only be surmised (Sellers et al., 1995). In the comparisons that follow, the model simulations are run with inputs that best represent the detailed, independent measurements of those inputs made at each site; on larger scales, more parameterization and generalization will be required. Fortunately, the TSTIM is not very sensitive to many of the parameters that are difficult to obtain on regional scales (see the section on the assessment of ancillary data requirements).

Database Description

The FIFE Database

The FIFE measurements used here were made at FIFE sites 16, 22, 24, and 26 [see Smith et al. (1992) for site descriptions]. Each of these sites was equipped with an automatic meteorological station (AMS) and either a Bowen ratio or eddy correlation system, where micrometeorological and flux measurements were recorded at 30-min intervals. The surface flux measurements made during the FIFE experiment are described by Kanemasu et al. (1992) and Smith et al. (1992). At each AMS, wind measurements were acquired at a height of 5.4 m, and air temperature was sampled at 2 m. The assumption that sensible heat increases linearly in time from a value of zero at 1 h past sunrise [Eq. (11)] is difficult to fulfill if short time-scale fluctuations in wind speed occur near time t_1 or t_2; in such cases, the resistance to sensible heat transport [Eq. (7)] becomes uncharacteristic of the time interval in question. Therefore, the wind speed data from the FIFE experiment have been averaged in time: the wind speed used at time t_1 was an average from $t_1 - 1$ h to t_2, and the wind speed used at time t_2 was an average from t_1 to $t_2 + 1$ h.

Data collected during each of the intensive field

campaigns (IFCs) 1–4, spanning from May to October 1987, are represented in our comparisons. This period encompasses the major phenological stages of the native prairie vegetation, from "green up" (IFC 1, late May) to senescence (IFC 4, early October). The TSTIM requires an accounting of both total LAI (live and dead) and the fraction of green vegetation; the total LAI is used in computing the weighting function $f(\varphi)$ in Eq. (6a), the soil boundary layer resistance, and the partitioning of net radiation between the soil and canopy regimes [Eq. (6e)], whereas only green vegetation contributes to the canopy transpiration rate [Eq. (6j)]. In accord with Norman et al. (1995b), green LAI values were used for IFCs 1–3 (assuming $f_g=1$); whereas, in IFC 4, when the vegetation was predominantly dormant, the total LAI was computed as

$$LAI_{total} \approx LAI_{green} + 0.5 \frac{dry\ weight_{dead}}{dry\ weight_{live}} LAI_{green} , \quad (19)$$

assuming that dead leaves contribute on average half the LAI per unit dry weight that live leaves do. The fraction of green vegetation for IFC 4 was then computed as LAI_{green}/LAI_{total}. For all IFCs, the surface roughness length was assumed to be $h_c/10$ (where h_c is the average canopy height) and displacement height, $2h_c/3$. The green LAI, dead and live dry weight, and canopy height data were obtained from the FIFE CD-ROM data collection (Strebel, et al., 1994).

In testing the TSM, Norman et al. (1995b) used surface brightness temperatures acquired with a helicopter-mounted radiometer hovering at a height of approximately 300 m above the ground. The nadir footprint of this system was approximately 5.2 m, thus effecting a spatial averaging over small-scale inhomogeneities in the landscape, which is beneficial to flux estimation algorithms. However, because these measurements were taken at irregular time intervals, they could not be used to test the TSTIM. Instead, we used surface temperature measurements obtained at selected AMS installations with Everest multiplexed infrared thermometers (IRTs), Model 4000. These thermometers were mounted approximately 2 m above the ground, yielding a nadir footprint 0.5 m diameter.

A comparison between IRT-measured surface temperature at sites 16, 24, and 26 and temperatures measured by the helicopter-mounted radiometer at the same sites and times (with atmospheric corrections applied) shows the IRT observations to be on average 3 C° colder than the helicopter observations (Fig. 4). A bias of similar magnitude was noted by Goetz et al. (1995), who suggest that it may be related to the difference in spatial sampling between the two instruments. The IRTs sample a smaller area of ground and thus, if positioned preferentially over a region with higher vegetation cover (away from footpaths and grazed areas), would register consistently cooler temperatures. This hypothesis is supported by the fact that the apparent bias is smaller during IFC 4
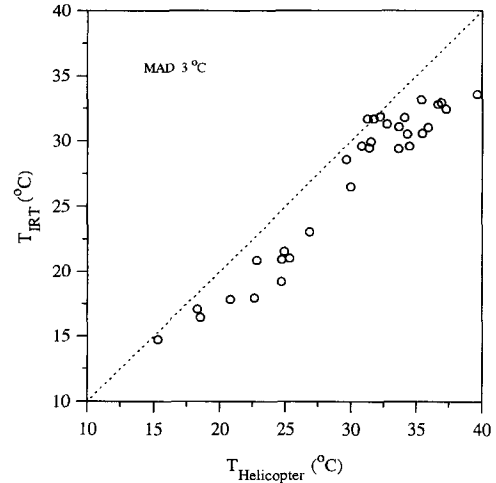

Figure 4. Surface radiometric temperature measurements from ground-based infrared thermometers at FIFE weather stations compared with helicopter-based measurements adjusted for intervening atmospheric effects. The ground-based measurements are used in the TSTIM, and the helicopter measurements were used in the TSM.

(the "senescence" period) when vegetation cover least affects the composite surface temperature. Additionally, the Model 4000 IRT does not perfectly correct for thermal emission from the thermometer itself and therefore is subject to error when the target and thermometer-body temperatures are not equal. Given that the air surrounding the IRT was consistently cooler than the surface during the times studied here, this error would cause temperatures measured with the Model 4000 IRT to be underestimated. Because this bias is constant in time, it proves to have little effect on flux estimates from the TSTIM, which is sensitive only to the *time change* in surface temperature (see the section comparing TSTIM estimates with observations).

Serial rawinsonde measurements of temperature, wind, and humidity in the PBL were acquired daily during all IFCs in the FIFE. The balloons were launched at the northern edge of the FIFE site, less than 15 km away from all subsites studied here.

The Monsoon '90 Database

The TSTIM has also been tested with data collected at METFLUX sites 1 and 5 in the Monsoon '90 experimental area. Site 1 is a shrub-dominated subwatershed in the Lucky Hills study area, whereas site 5, in the Kendall subwatershed, is primarily a grass ecosystem. The vegetation cover at both sites is sparse (LAI=0.4 and 0.8 at sites 1 and 5, respectively) and heterogeneous in type and height. The data used here were collected between 28 July and 10 August 1990, when both sites were near peak greenness ($f_g=1$ was used at both sites). During this time, several rainfall events occurred, so a variety of soil

Table 1. Definition of Quantitative Measures Used to Evaluate the Performance of the TSTIM

Measure	Description	Computational Form
N	Number of observations	
$\overline{O}$	Mean of the observed variable	$\dfrac{1}{n}\sum_{i=1}^{n} O_i$
$\overline{P}$	Mean of the model predicted variable	$\dfrac{1}{n}\sum_{i=1}^{n} P_i$
S_o	Standard deviation of the observed variable	$\left[\dfrac{1}{n-1}\sum_{i=1}^{n}(O_i-\overline{O})^2\right]^{1/2}$
S_p	Standard deviation of the predicted variable	$\left[\dfrac{1}{n-1}\sum_{i=1}^{n}(P_i-\overline{P})^2\right]^{1/2}$
a, b	Intercept and slope of the linear regression of P on O	$\hat{P}_i=a+bO_i$
MAD	Mean absolute difference	$\dfrac{1}{n}\sum_{i=1}^{n}|P_i-O_i|$
RMSD	Root mean square difference	$\left[\dfrac{1}{n}\sum_{i=1}^{n}(P_i-O_i)^2\right]^{1/2}$
RMSD$_s$	Systematic root mean square difference	$\left[\dfrac{1}{n}\sum_{i=1}^{n}(\hat{P}_i-O_i)^2\right]^{1/2}$
RMSD$_u$	Unsystematic root mean square difference	$\left[\dfrac{1}{n}\sum_{i=1}^{n}(P_i-\hat{P}_i)^2\right]^{1/2}$
r^2	Coefficient of determination	$\left[\sum_{i=1}^{n}(P_i-\overline{P})(O_i-\overline{O})^2\right]\Big/\left[\sum_{i=1}^{n}(O_i-\overline{O})\right]^2\sum_{i=1}^{n}(P_i-\overline{P})^2$

moisture conditions were sampled. Measurements of wind speed and air temperature were made at heights of 4.3 m and 4 m, respectively. The wind speeds used in the resistance calculations [Eq. (7)] were time-averaged values obtained as described earlier for the FIFE tests. Surface fluxes used here for comparison with estimated fluxes were computed by using the variance method described by Tillman (1972); Kustas et al. (1994a) showed that this method yields flux estimates that are on average within 20% of those obtained through standard eddy correlation techniques. This level of variability is typical of other flux estimation techniques (Dugas et al., 1991; Nie et al., 1992) and thus is deemed acceptable.

The canopy architecture parameters used here are identical with those used by Norman et al. (1995b). Because the vegetation at both sites is so heterogeneous in height and cover, specifying an appropriate "average vegetation height" is difficult; therefore, the displacement heights estimated independently for Walnut Gulch by Kustas et al. (1994a) are used to compute an effective height at each site. Because the canopy cover was relatively sparse and open, it is assumed that $h_c=2d$, instead of the typical $h_c=3d/2$ relation. For site 1, the values $z_m=0.04$ m, $d=0.4$ m, and $h_c=0.8$ m, were used; and, for site 5, $z_m=0.01$ m, $d=0.3$ m, and $h_c=0.6$ m.

Special effort was taken during the Monsoon '90 experiment to assure that ground-based measurements of surface brightness temperature were not biased by the small-scale inhomogeneity in the landscape. At each site,

fiducial soil and vegetation temperatures were sampled continuously with two stationary Everest Interscience radiometers (Models 110 and 4000), one pointed at bare soil and the other at a representative part of the canopy. Periodically, measurements were made with similar instruments mounted on yokes and carried over a set of prescribed transects within the site [see Moran et al. (1994) for details concerning the yoke measurements]. Regression coefficients were then computed by using the yoke measurements as the dependent variable and the canopy and soil temperatures as independent variables. With these coefficients, continuous estimates of a spatially representative composite temperature can be constructed from the in situ component temperature measurements.

Radiosonde instruments were launched at site 1 on four different days during the Monsoon campaign. The earliest soundings, however, occurred at approximately 8:00 A.M. MST, 1.5 h after the first observation of radiometric surface temperature used by the TSTIM. By this time, the mixed layer was already noticeably developed and the simple PBL model described earlier did not perform well with the use of these profiles. Therefore, 12:00 h UTC (5:00 A.M. MST) soundings from the nearest radiosonde network station (at Tucson, approximately 60 km from Walnut Gulch) were used instead. A first-order correction for adiabatic cooling due to the elevation difference, $\Delta Elev$, between Tucson (elevation 800 m above sea level) and Walnut Gulch (elevation 1500 m)
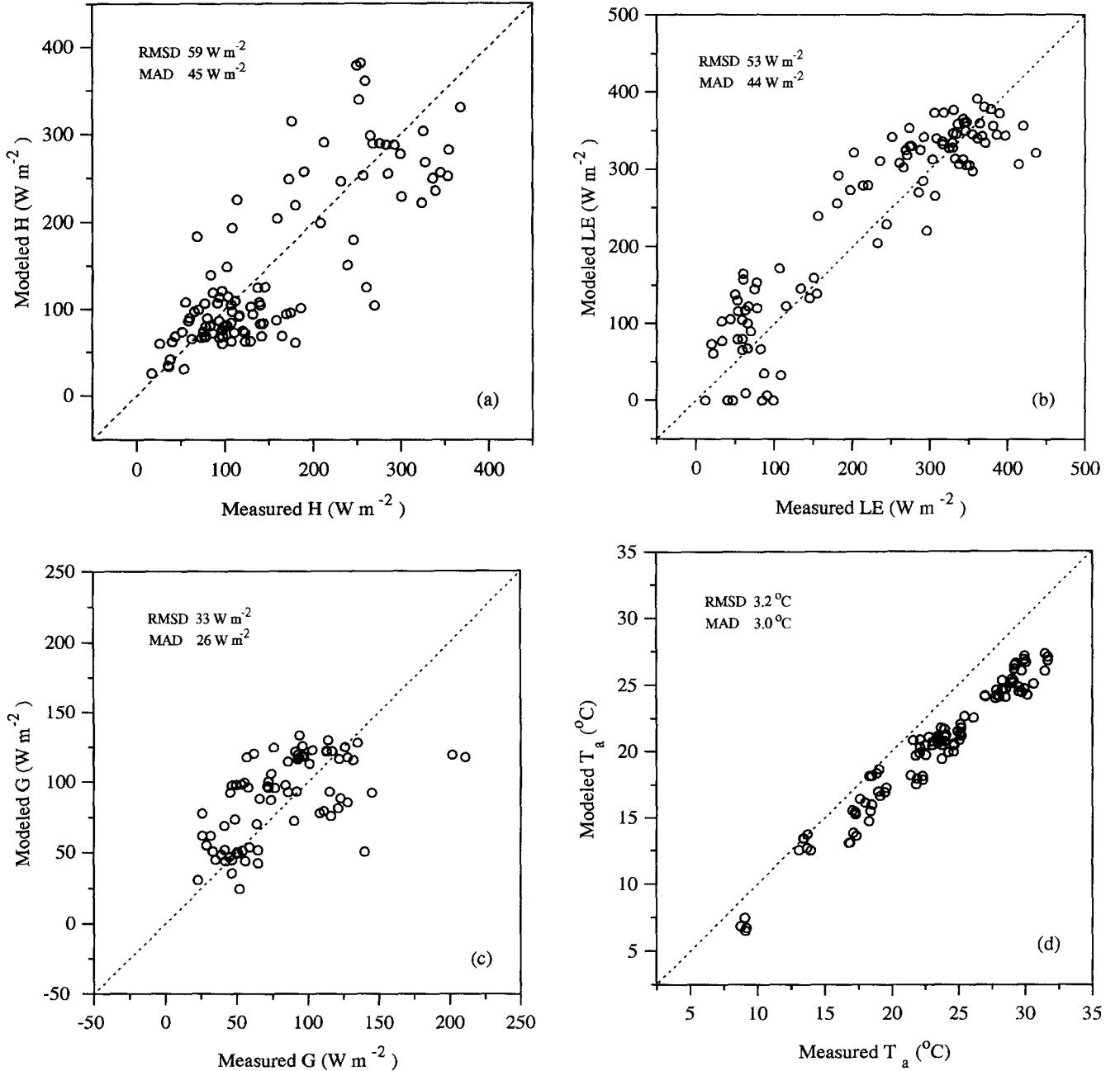
Figure 5. Comparison of TSTIM predictions at 5.5 h after sunrise of (a) sensible heat flux, (b) latent heat flux, (c) soil heat conduction flux, and (d) air temperature at 2 m with micrometeorological measurements from FIFE.

may be expressed as

$$T(z)_{\text{corr}} = T(z)_{\text{Tucson}} - \Delta Elev \Gamma_{\text{d}} \left(\frac{z_{\text{max}} - z}{z_{\text{max}}} \right) , \qquad (20)$$

where $T(z)_{\text{Tucson}}$ is the absolute temperature in K in the Tucson sounding at height z and Γ_{d} is the dry adiabatic lapse rate ($\sim$1 K 100 m^{-1}). Streamlines at greater altitudes within the profile will be less affected by elevation, so the application of this correction is constrained to heights below some maximum value, z_{max} (we use 4000

m). As is demonstrated in the next section, this correction proves to have little effect on the flux estimates generated by the TSTIM.

Comparison of TSTIM Estimates with Observations
The validity of the TSTIM has been evaluated by using the quantitative measures of model performance suggested by Willmott (1982). These measures and their computational forms are listed in Table 1 and include the mean absolute difference (MAD), and the root mean square difference (RMSD), along with its systematic and

Table 2. Quantitative Measures of Model Performance with the FIFE Database

Flux	N	$\overline{O}$	$\overline{P}$	S_o	S_p	a	b	MAD	RMSD	RMSD$_s$	RMSD$_u$	r^2
Instantaneous		W m^{-2}	W m^{-2}	W m^{-2}	W m^{-2}	W m^{-2}		W m^{-2}	W m^{-2}	W m^{-2}	W m^{-2}	
H	102	155	146	93	93	20	0.81	45	59	20	55	0.65
LE	100	221	235	129	123	41	0.88	44	53	21	49	0.84
G	75	81	88	39	30	51	0.46	26	33	22	24	0.34
Daytime		MJ m^{-2}	MJ m^{-2}	MJ m^{-2}	MJ m^{-2}	MJ m^{-2}		MJ m^{-2}	MJ m^{-2}	MJ m^{-2}	MJ m^{-2}	
$\langle H \rangle$	89	3.7	3.0	2.2	2.1	0.29	0.74	1.2	1.6	0.9	1.3	0.61
$\langle LE \rangle$	71	8.2	8.4	4.9	4.4	1.5	0.84	1.3	1.6	0.8	1.4	0.90
$\langle G \rangle$	65	1.8	2.5	1.0	1.2	1.1	0.79	0.9	1.1	0.8	0.8	0.48

Analyses for both instantaneous and daytime total flux estimates are given.

unsystematic components (RMSD$_s$ and RMSD$_u$, respectively). Willmott (1981, 1982) demonstrated how members of this statistical suite can be combined to generate additional useful measures; for example, the mean bias between estimated and observed fluxes is given by $\overline{P}-\overline{O}$, and the proportion of the total RMSD arising from systematic biases is reflected in the quantity RMSD$_s^2$/RMSD^2.

To assess the change in performance elicited by the introduction of a time-integrated component to the original two-source model, both the TSTIM and TSM have been run with identical input databases from the FIFE and Monsoon '90 field experiments. We limit the following discussion to comparisons between model predictions and observations at time t_2 (5.5 h past sunrise) only, because of the high relative errors typically associated with early morning flux measurements.

Figure 5 compares heat fluxes measured during the FIFE campaign with those predicted by the TSTIM; quantitative measures of these comparisons are given in Table 2. The level of agreement between modeled and measured latent heat fluxes (Fig. 5b) is comparable to the variability observed among the measurements themselves; in an intercomparison of LE measurements obtained with different flux systems during FIFE '87, Nie et al. (1992) found differences of 20%, on average, whereas the mean model deviation, RMSD/$\overline{O}$, from Table 2 is 24%. The scatter between modeled and measured fluxes of sensible heat (Fig. 5a) is somewhat larger, with an RMSD/$\overline{O}$ value of 38%. However, as noted by Norman et al. (1995b), the average Bowen ratio associated with the latent heat measurements considered by Nie et al. (1992) was 0.5, suggesting a variation of as much as 40% among measurements of sensible heat in FIFE '87. The scatter in Figure 5a increases at high heating rates, owing in part to the difficulty in estimating the fraction of green vegetation present during IFC 4, when most of the vegetation had senesced.

Model estimates of air temperature are well correlated with measurements from FIFE but show a negative bias of 3 C° (Fig. 5d), identical in magnitude with the instrumental bias suspected in the IRT surface tempera-

ture measurements used to drive the model (Fig. 4). This behavior suggests that this bias in surface temperature is being absorbed into the computed air temperatures, leaving the true difference $T_a - T_{RAD}$ intact.

Experimentation with the TSTIM shows that this is indeed the case. Figure 6a and b shows the effect of a simulated time-independent bias in surface brightness temperature. The results from two sets of model runs are compared here: in one set, the radiometric temperatures at both sampling times, $T_{RAD,1}$ and $T_{RAD,2}$, were increased uniformly by 5 C°, simulating a large constant bias; in the other set, the temperatures were unmodified. The TSTIM responded to this bias by offsetting its air temperature estimates by an equal amount ($\overline{O}-\overline{P}$ in Fig. 6b is 4.9 C°), leaving the surface-to-air temperature difference, and thus the sensible heat flux estimates, essentially unaltered (Fig. 6a). An increase in $\Delta T_{RAD} = T_{RAD,2} - T_{RAD,1}$, however, is correctly interpreted as a signal of increased time-integrated sensible heating, as is demonstrated in Figure 6c and d. Here the radiometric temperature at the second observation time only was artificially increased by 3 C°. Figure 6d shows that the air temperature estimates are not significantly affected by this experiment—the increased ΔT_{RAD} translates purely into an increase in time-integrated sensible heating (Fig. 6c).

Figure 6 demonstrates one of the great strengths of the TSTIM. Because the model uses time differences in surface temperature, rigorous temperature calibration is unnecessary as long as the corrections are additive and do not vary significantly over the time interval in question. The TSM performs quite poorly when applied to this same database, yielding RMSD and MAD values for H and LE twice those obtained with the TSTIM. When the FIFE IRT measurements are corrected for the 3 C° bias apparent in Figure 4, the TSM produces results very similar to those shown in Figure 5.

Figure 7a–c compares observed and modeled sensible, latent, and ground heat fluxes from the Monsoon '90 campaign; quantitative comparisons are provided in Table 3. Estimates computed both with and without the atmospheric lapse rate correction for site elevation given in Eq. (20) are shown to demonstrate that its effect is
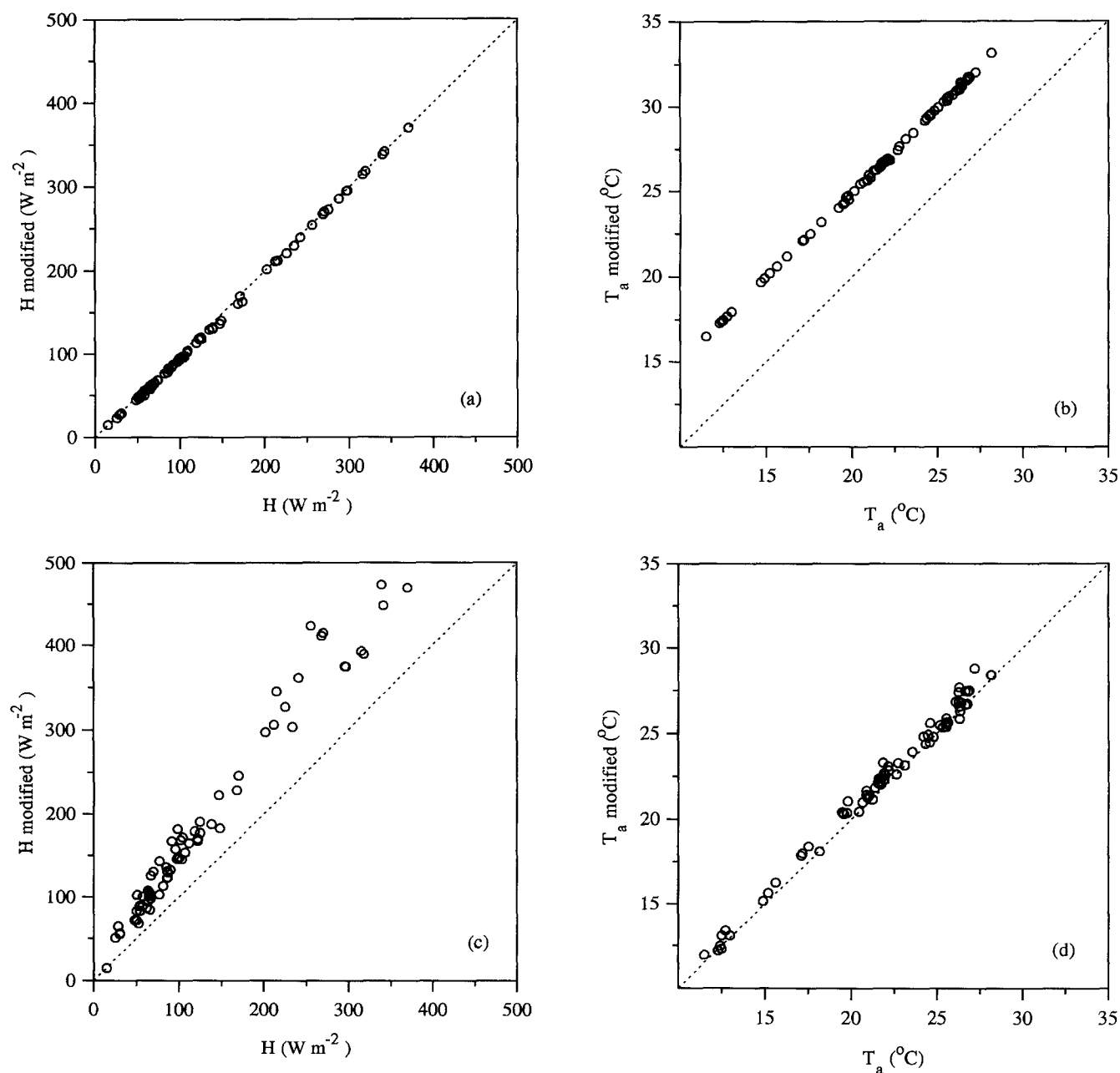
Figure 6. TSTIM predictions of (a) sensible heat and (b) air temperature at 2m with the use of modified FIFE data, where 5 C° have been added to the brightness temperatures at both observation times, vs values predicted from the actual brightness temperatures. Analogous comparisons are shown in (c) and (d) for simulations where 3C° have been added to the surface radiometric temperature at the second observation time only (no bias in temperature at the first observation time).

minimal. This correction (about 2 K km^{-1}) improves model agreement with measured fluxes slightly yet alters flux estimates by less than 5% on average. In this case, the use of a nonlocal temperature sounding does not significantly degrade the modeled fluxes; this bodes well for the practical utility of the TSTIM.

The RMSD values computed for these quantities are improved over those obtained by the TSM: the TSTIM (with the lapse rate correction) yields RMSD values for

H and LE of 32 and 40 W m^{-2}, respectively, whereas the TSM yields values of 44 and 58 W m^{-2}. Whereas TSM estimates of sensible heat flux are biased low by 28 W m^{-2}, the TSTIM overestimates H by only 7 W m^{-2} on average. Both models yield very similar estimates of G.

The correlation between modeled and measured air temperatures for Monsoon '90 is somewhat worse than that achieved in the FIFE simulations (see Fig.7d), but the average fractional deviation, RMSD/O, is comparable
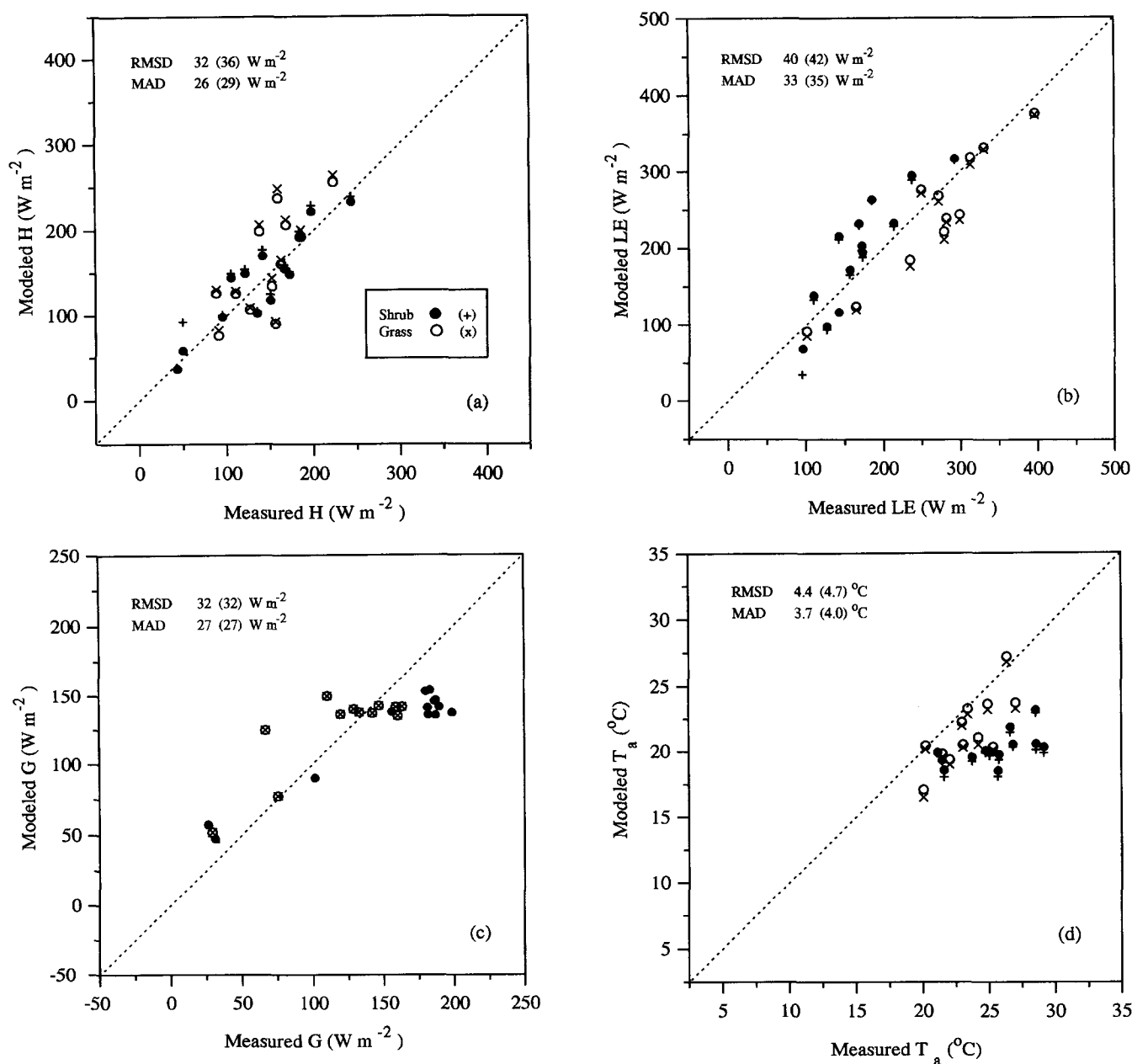
Figure 7. Comparison of TSTIM predictions at 5.5 h after sunrise of (a) sensible heat flux, (b) latent heat flux, (c) soil heat conduction flux, and (d) air temperature at 4 m with micrometeorological measurements from Monsoon '90. Results obtained both with (site 1, solid circles; site 5, open circles) and without (site 1, +; site 5, ×) the atmospheric lapse rate correction for site elevation given in Eq. (20) are shown; uncorrected results are designated with parentheses.

(about 15%). Estimated air temperatures at site 1 (the low-LAI, shrub-dominated site) are biased low by 5 C°, whereas site 5 (the grass-dominated site) shows a lesser bias of 2 C°. The origin of these biases is unclear; the surface brightness temperature measurements made during the Monsoon '90 campaign were much less vulnerable to inhomogeneities in the landscape than were the FIFE ground-based measurements. The discrepancies between modeled and measured air temperatures may be due to a combination of small individual errors, both

in the measurements and in our description of the system. They may be related, in part, to biases inherent in the Model 4000 IRT, to advection effects (which are currently neglected in the TSTIM), or to residual corrections required to translate the atmospheric sounding obtained at Tucson to the Walnut Gulch site that are not accomplished through the simple approximation Eq. (20). Whatever the causes, they do not appear to significantly affect the Monsoon '90 flux estimates.

A method for extrapolating from instantaneous esti-

Table 3. Quantitative Measures of Model Performance with the Monsoon '90 Database

Flux	N	$\overline{O}$	$\overline{P}$	S_o	S_p	a	b	MAD	RMSD	RMSD$_s$	RMSD$_u$	r^2
Instantaneous		W m^{-2}	W m^{-2}	W m^{-2}	W m^{-2}	W m^{-2}		W m^{-2}	W m^{-2}	W m^{-2}	W m^{-2}	
H	25	143	156	48	58	19	0.97	29	36	14	33	0.65
H_{corr}	25	143	150	48	58	9	0.99	26	32	7	32	0.69
LE	24	214	211	81	85	17	0.91	36	42	8	41	0.76
LE_{corr}	24	214	218	81	82	28	0.89	33	40	10	39	0.77
G	25	137	126	54	33	55	0.52	27	32	28	16	0.74
G_{corr}	25	137	126	54	33	55	0.52	27	32	28	16	0.74
Daytime		MJ m^{-2}	MJ m^{-2}	MJ m^{-2}	MJ m^{-2}	MJ m^{-2}		MJ m^{-2}	MJ m^{-2}	MJ m^{-2}	MJ m^{-2}	
$\langle H_{corr} \rangle$	20	4.1	3.5	1.2	1.5	-0.7	1.01	0.8	1.0	0.6	0.8	0.68
$\langle LE_{corr} \rangle$	17	6.3	6.6	1.5	2.2	-2.0	1.35	0.9	1.0	0.6	0.8	0.86
$\langle G_{corr} \rangle$	24	3.1	3.4	1.3	0.8	1.6	0.58	0.5	0.7	0.6	0.3	0.89

Analyses for both instantaneous and daytime total flux estimates are given. All runs use atmospheric soundings acquired in Tucson; the subscript "corr" indicates results obtained when these soundings are corrected for the difference in elevation between Tucson and Walnut Gulch [Eq. (20)].

mates of energy flux to daytime totals was presented in an earlier section. Figure 8a–c shows the results of this extrapolation for the FIFE data set, using evaporative fractions [Eq. (18)] calculated from TSTIM estimates of LE_2 and G_2 and measured values of $R_{n,2}$. Analogous figures for Monsoon '90 are shown in Figure 9a–c. In these extrapolations, "daytime" has been defined as the time interval during which net radiation exceeds 50 W m^{-2} and is approximately 12 h in duration on average for the days studied here. This limit is imposed to exclude measurements at low flux levels that typically have high relative errors. Furthermore, the simple parameterization for G in Eq. (6k) does not realistically reproduce true soil heat conduction curves early and late in the day, owing to diurnal phase and curve-shape differences between G and R_n (Choudhury et al., 1987).

Tables 2 and 3 list quantitative measures of the comparison between modeled and measured daytime fluxes for the FIFE and the Monsoon '90 databases, respectively. The relative scatter among observed and estimated daytime total fluxes in each case is similar to that achieved with instantaneous flux estimates. RMSD values for Monsoon '90 daily flux estimates are approximately 1 MJ m^{-2} and, for FIFE, between 1 and 2 MJ m^{-2}; these values are consistent with uncertainties in previous studies (Brutsaert and Sugita, 1992; Kustas et al., 1994b; Norman et al., 1995a). Some of the scatter in Figures 8 and 9 is induced by intermittent cloud cover, which can violate the notion of a "self-preserving" energy budget. Further restricting the definition of "daytime" to higher limits in net radiation would significantly improve the agreement with measured daytime fluxes, primarily by excluding time intervals where Eq. (6k) for G fails most acutely.

ASSESSMENT OF ANCILLARY DATA REQUIREMENTS

Parameter Sensitivity: A Comparison with the TSM

A list of all ancillary measurements and parameters required by the TSTIM is given in Table 4. In this table,

we also list a measure of how sensitive TSM and TSTIM estimates of sensible heat are to uncertainties in each of these input quantities. In accord with Zhan et al. (1996), the relative sensitivity, S_p, of a model flux estimate to $X\%$ uncertainties in a parameter p can be expressed as

$$S_p(X\%) = \left| \frac{H_- - H_+}{H_0} \right|, \qquad (21)$$

where H_0, H_+, and H_- are the fluxes predicted when p equals its reference value p_0, $p_+ = p_0(100+X)\%$, and $p_- = p_0(100-X)\%$, respectively, and all other parameters are held at their reference values. These sensitivity values aid in assessing the accuracy with which input parameters must be specified to attain a target level of uncertainty in model predictions. However, Zhan et al. (1996) point out that the S_p value computed for a given parameter may depend on the choice of reference value for that parameter, so the sensitivities listed in Table 4 should be considered approximate assessments. The reference values used in this sensitivity study are listed in Table 4. The values for parameters common to both the TSM and the TSTIM are those used by Zhan et al. (1996), representing median values in their test case suite.

In a comparison of four surface temperature-based flux estimation models, Zhan et al. (1996) found that the TSM showed the best agreement with flux measurements acquired during field experiments conducted in Kansas, Arizona, and Oklahoma. Some models performed better than others in various vegetative regimes, but the TSM performed well consistently and required no empirical tweaking of input parameters from region to region. Furthermore, the study found that the TSM "required relatively few parameters and is not very sensitive to the uncertainties in the estimates of most parameters."

Table 4 shows that the TSTIM is similarly or less sensitive than the TSM to input parameters common to both models. Note, in particular, the dramatic decrease in sensitivity to errors in radiometric temperature. Two scenarios concerning the time behavior of the assumed error in T_{RAD} are presented in Table 4: one in which the
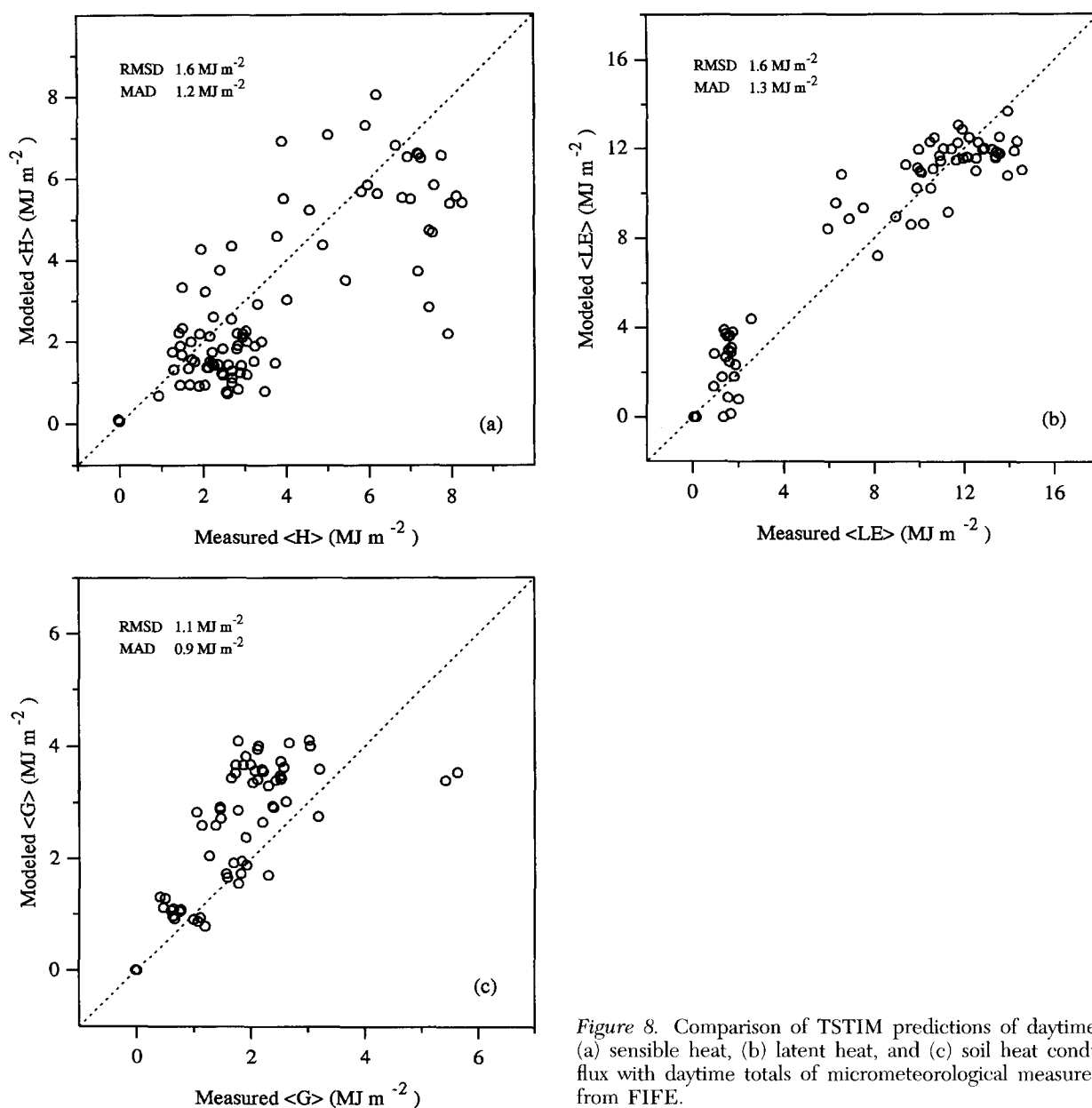
Figure 8. Comparison of TSTIM predictions of daytime total (a) sensible heat, (b) latent heat, and (c) soil heat conduction flux with daytime totals of micrometeorological measurements from FIFE.

error is multiplicative (a scaling error) and the other in which the error is an additive bias, constant in time. The TSM does not utilize time change information and thus cannot distinguish between these scenarios—10% variations in surface temperature yield roughly 50% variations in sensible heating estimates in each case. The TSTIM estimates of sensible heat are affected by only 16% if the error is multiplicative and by 2% if it is a constant bias.

The decision to replace the need for ancillary air temperature measurements with specifications of atmospheric lapse rate appears to be a prudent one. Estimates of local air temperature acquired through interpolation to the satellite image grid will often be uncertain by at least 10% (see Fig. 1), translating into 40% uncertainties in TSM flux estimates. The local atmospheric temperature profile may be similarly difficult to characterize;

however, the TSTIM is relatively insensitive to fairly large uncertainties in lapse rate specification.

Applying the TSTIM on a Regional Scale

The TSTIM was tested with data collected during two field experiments and was found to perform well on the 10–100 m scale in a variety of vegetative regimes. This model also has significant potential for application on regional scales because it requires minimal ground-based input and is insensitive to many biases that typically plague satellite measurements of surface temperature. In such an application, many of the input parameters listed in Table 4 would need to be obtained remotely; a strategy for acquiring these data is briefly outlined below.

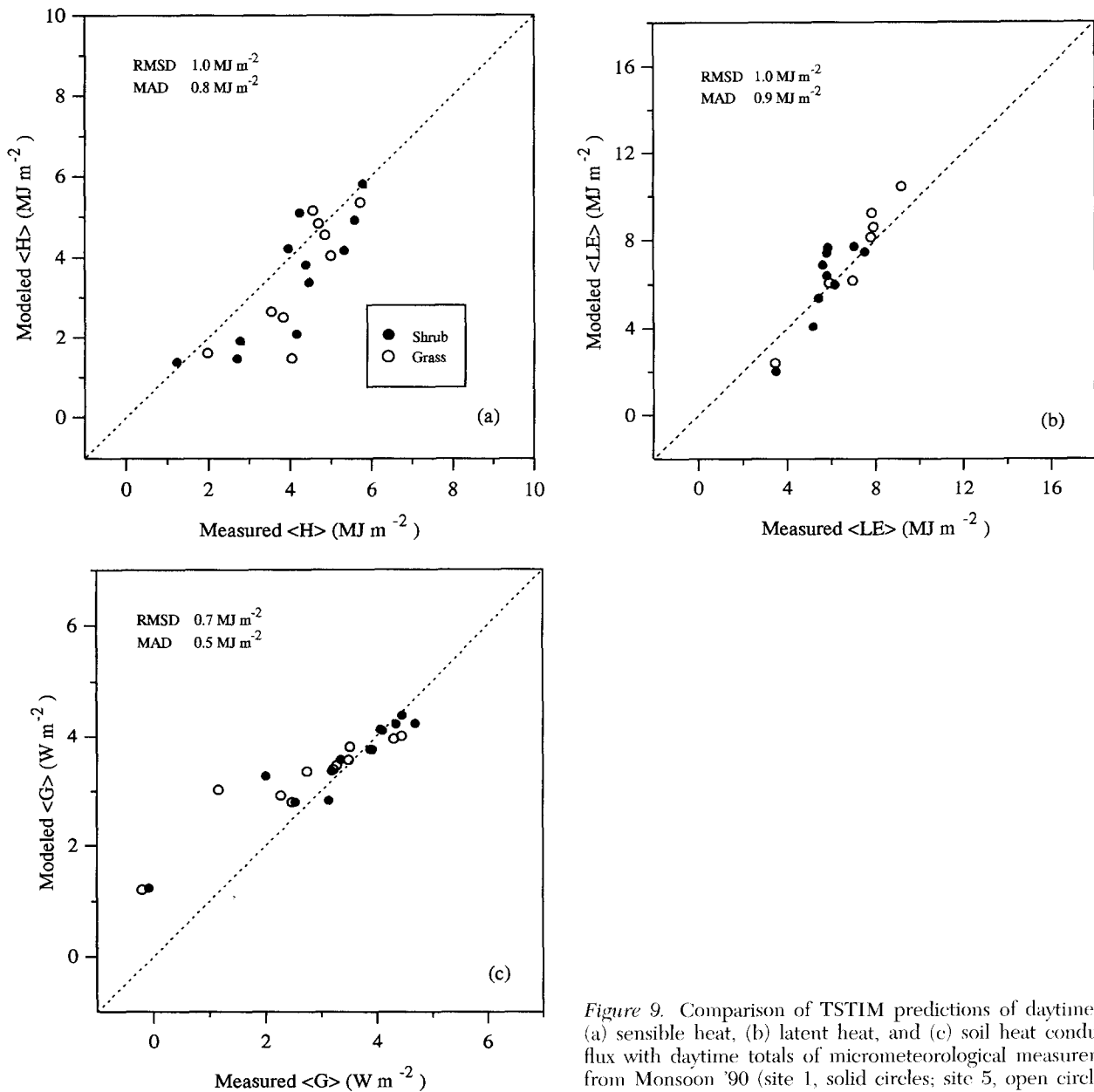The correlation between green LAI and the normalized difference vegetation index (NDVI) has been well

Figure 9. Comparison of TSTIM predictions of daytime total (a) sensible heat, (b) latent heat, and (c) soil heat conduction flux with daytime totals of micrometeorological measurements from Monsoon '90 (site 1, solid circles; site 5, open circles).

studied (Carlson et al., 1990; Baret and Guyot, 1991; Hall et al., 1992). Sellers et al. (1994) detail methods for obtaining green LAI from an adjusted NDVI product. Total LAI and the canopy greenness fraction, f_g, may then be estimated from the seasonal evolution in green LAI. The success with which these methods predict vegetation biophysical parameters has yet to be evaluated; however, comparisons can be made against data collected during field experiments such as FIFE. A good estimate of f_g is important for accurate partitioning of the energy budget, because it accounts for senescent vegetation that contributes to the canopy sensible heat flux, H_c, but not to the latent heat flux, LE_c. As was observed with the TSM (Zhan et al., 1996), the TSTIM becomes more sensitive to uncertainties in f_g as the green fraction increases.

It is possible to infer other vegetation characteristics (vegetation height, h_c, and average leaf size, s) from a map of NDVI if the predominant type of vegetation in each pixel is known. This type of information is now becoming available in the form of continental-scale land-cover classification maps; the 1990 Conterminous U.S. Landcover Characteristics Data Set developed by the U.S. Geological Survey (USGS) Earth Resources Observation Systems (EROS) Data Center is one such example. This data set includes a classification of seasonal land cover types for 1990 at a resolution of 1 km. In vegetated regions, surface roughness length and displacement height can be parameterized in terms of fractional canopy height (Shaw and Pereira, 1982); in nonvegetated regions, some fixed value of z_m may need to be assumed.

Table 4. Sensitivity of TSM and TSTIM Estimates of Sensible Heat Flux to Uncertainties in Model Input Parameters.

Parameter and Nominal Value		TSM	TSTIM		
p	p_o	$S_p(10\%)$	$S_p(10\%)$	$S_p(25\%)$	$S_p(75\%)$
$T_{RAD,1,2}$ (mult)	24, 34 °C	0.52	0.16	0.40	1.19
$T_{RAD,1,2}$ (add)	24, 34 °C	0.52	0.02	0.06	0.19
$T_{a,1,2}$	21, 26 °C	0.43	0	0	0
u	4 m/s	0.06	0.05	0.12	0.35
h_c	0.6 m	0.07	0.07	0.19†	
d	0.39 m	0.05	0.05	0.12†	
z_m	0.06 m	0.00°	0.01	0.03	0.06
F	1.0	0.07	0.03	0.08	0.27
$f(\varphi=0)$	0.39	0.04	0.05	0.12	0.42
s	0.005 m	0.01	0.01	0.04	0.14
f_g	0.5	0.07	0.07	0.17	0.52
a_{PT}	1.3	0.08	0.07	0.17	0.52
κ	0.45	0.07	0.06	0.14	0.43
z_i	50 m	0	0.01	0.03	0.08
$d\theta_i/dz$	~4 Kkm^{-1}	0	0.01	0.03	0.09

Note: The sensitivity, S_p ($X\%$) [Eq. (21)], to $X\%$ uncertainties in the parameter p is tabulated for both models, assuming a nominal value for the parameter of p_o. For the parameter T_{RAD}, two types of uncertainties are considered: a multiplicative bias (mult) and an additive bias (add); see text for further discussion.
° The value is less than 0.005.
† Computed for 20% variation in p to avoid conflict with other parameters.

When h_c, z_m, and d scale together, the TSTIM is significantly less responsive to variations in assumed canopy height; the sensitivity to 50% uncertainties in h_c in this case is only 0.02.

Wind speed will have to be interpolated between surface synoptic network measurements. Fortunately, wind speed at a height of 10 m (the standard weather station measurement height) is a fairly conservative quantity on the synoptic scale; the wind at this height is driven primarily by horizontal pressure gradients and is largely decoupled from local surface characteristics. The 5 h time average in wind speed required by the TSTIM further reduces errors due to interpolation.

The boundary layer component of the TSTIM can be initialized with 12:00 UTC soundings from the radiosonde network, interpolated between stations with the aid of a mesoscale forecast model. The sensitivity tests discussed in the preceding section indicate that relatively large errors in lapse rate can be tolerated.

Although single-parameter sensitivity analyses are enlightening in comparing different models, a more realistic assessment of model sensitivity must allow for uncertainties in multiple input parameters. The probable error in sensible heating provoked by random errors in several input parameters can be estimated by running an ensemble of simulations in which these parameters are corrupted with Gaussian noise and then computing the standard deviation in modeled H over this ensemble. The TSTIM input parameters that will be most difficult to obtain remotely are wind speed, roughness length, displacement height, leaf area index, the fraction of green vegetation, leaf size, and atmospheric lapse rate. Simulating 25% errors in each of these parameters yields a probable error of 16% in sensible heating. Clearly, random errors in many of the input parameters to the TSTIM tend to cancel themselves out, resulting in a lower net error in the predicted flux.

CONCLUSIONS

A potentially powerful method for using thermal infrared remote sensing techniques to diagnose the partitioning in the earth's surface energy budget has been presented. A series of simple analytical expressions have been assembled that describe the transport of sensible heat from a vegetated land surface to the overlying planetary boundary layer as the surface heats during the morning hours. These surface energy balance equations serve as a lower boundary constraint for a simple model of planetary boundary evolution, describing growth and heating in the PBL in response to this time-integrated influx of heat.

The primary strength of this approach, regarding its potential for remote applications, is that it requires minimal ground-based input. In particular, the need for ancillary measurements of local air temperature, required by most thermal infrared flux models, has been eliminated; near-surface air temperature is computed as a boundary condition common to both the surface and the boundary layer components of the model. Furthermore, because the model uses the time differential in brightness temperature, it is relatively insensitive to time-independent

biases inherent in infrared satellite observations of the earth's surface. This reduces the need for high accuracy in sensor calibration, in atmospheric corrections to surface brightness, and in the specification of surface emissivity. The effect of sensor view angle on apparent surface temperature is explicitly built into the model; thus radiometric temperatures obtained at any view angle can be used to drive the model. This feature increases the feasibility of using TIR observations from geosynchronous satellites and other remote instruments with off-nadir sensor viewing angles.

The TSTIM has been tested with data collected during the FIFE and Monsoon '90 campaigns and was found to perform well over both well-vegetated and sparsely vegetated surfaces. Comparisons between modeled and measured fluxes from both experiments yield differences comparable to those achieved by models that do require air temperature as an input and to errors typical of the flux measurement methods themselves.

The TSTIM can be enhanced with further modification. Specifically, a more detailed model of boundary layer development may eventually replace the simple area-integral method described in Eq. (10). Simple algorithms for estimating the effects of advection and subsidence are available (Diak and Whipple, 1993) and can easily be incorporated. As noted by Norman et al. (1995b), assumptions concerning canopy transpiration rate (here, the Priestly-Taylor approximation is used) are not required if brightness temperature measurements at multiple view angles are available, such as those provided by the along track scanning radiometer. Alternatively, a simple biophysical model linking canopy transpiration with carbon assimilation can be implemented; however, this requires an additional observational input of near-surface vapor pressure (Norman et al. 1996). Finally, the accuracy of flux estimates may be improved by using more than two observations of surface temperature; averaging over several observations would lessen sensitivity to short time-scale fluctuations which may occur inopportunely during a single observation. The GOES-8 imager, for example, provides updated thermal infrared images every 15 min.

The feasibility of implementing the two-source time-integrated model on the regional or continental scale is a topic of ongoing study. Methods from the literature for specifying vegetation cover and type from satellite observations are being assessed; in particular, a reliable means of deducing the fraction of dormant vegetation in the scene must be developed to assure accurate partitioning of canopy fluxes. Sensitivity tests reported in this paper, however, suggest that the TSTIM is not overly sensitive to uncertainties in the input quantities that will be most difficult to obtain remotely.

REFERENCES

Anton, J. A., and Ross, J. K. (1987), Emissivity of the vegetation-soil system. *Sov. J. Remote Sens.* 5:49–55 (in Russian with English Summary).

Baret, F., and Guyot, G. (1991), Potentials and limits of vegetation indices for LAI and APAR assessment. *Remote Sens. Environ.* 35:161–173.

Becker, F., and Li, Z.-L. (1990), Temperature-independent spectral indices in thermal infrared bands. *Remote Sens. Environ.* 32:17–33.

Brutsaert, W. (1982), *Evaporation into the Atmosphere: Theory, History and Applications.* D. Reidel, Hingham, MA.

Brutsaert, W., Hsu, A. Y., and Schmugge, T. (1993), Parameterization of surface heat fluxes above forest with satellite thermal sensing and boundary layer soundings. *J. Appl. Meteorol.* 32:909–917.

Brutsaert, W., and Sugita, M. (1992), Application of self-preservation in the diurnal evolution of the surface energy budget to determine daily evaporation. *J. Geophys. Res.* 97:18,377–18,382.

Carlson, T. N. (1986), Regional-scale estimates of surface moisture availability and thermal inertia using remote thermal measurements. *Remote Sens. Rev.* 1:197–247.

Carlson, T. N., Dodd, J. K., Benjamin, S. G., and Cooper, J. N. (1981), Satellite estimation of the surface energy balance, moisture availability and thermal inertia. *J. Appl. Meteorol.* 20:67–87.

Carlson, T. N., Perry, M. P., and Schmugge, T. J. (1990), Remote estimation of soil moisture availability and fractional vegetation cover for agricultural fields. *Agric. For. Meteorol.* 52:45–69.

Choudhury, B. J., Idso, S. B., and Reginato, R. J. (1987), Analysis of an empirical model for soil heat flux under a growing wheat crop for estimating evaporation by an infrared-temperature based energy balance equation. *Agric. For. Meteorol.* 39:283–297.

Cooper, H. J., Smith, E. A., and Crosson, W. L. (1995), Limita-

tions in estimating surface sensible heat fluxes from surface and satellite radiometric skin temperatures. *J. Geophys. Res.* 100:25,419–25,427.

Deardorff, J. W. (1967), Empirical dependence of the eddy coefficient for heat upon stability above the lowest 50 m. *J. Appl. Meteorol.* 6:631–643.

Diak, G. R., and Whipple, M. S. (1993), Improvements to models and methods for evaluating the land-surface energy balance and "effective" roughness using radiosonde reports and satellite-measured "skin" temperatures. *Agric. For. Meteorol.* 63:189–218.

Diak, G. R., and Whipple, M. S. (1995), A note on estimating surface sensible heat fluxes using surface temperatures measured from a geostationary satellite during FIFE 1989. *J. Geophys. Res.* 100:25,453–25,461.

Dugas, W. A., Fritschen, L. J., Gay, L. W., Held, A. A., Matthais, A. D., Reichosky, D. C., Steduto, P., and Steiner, J. L. (1991), Bowen ratio, eddy correlation, and portable chamber measurements of sensible and latent heat flux over irrigated spring wheat. *Agric. For. Meteorol.* 56:1–20.

Gash, J. H. C. (1987), An analytical framework for extrapolating evaporation measurements by remote sensing surface temperature. *Int. J. Remote Sens.* 8:1245–1249.

Goetz, S. J., Halthore, R. N., Hall, F. G., and Markham, B. L. (1995), Surface temperature retrieval in a temperate grassland with multiresolution sensors. *J. Geophys. Res.* 100:25, 397–25,410.

Gurney, R. J., Hsu, A. Y. (1990), Relating evaporative fraction to remotely sensed data at the FIFE site. In *Symposium on FIFE: First ISLSCP Field Experiment*, February 7–9, 1990, American Meteorological Society, 112–116, Boston, MA.

Hall, F. G., Huemmrich, K. F., Goetz, S. J., Sellers P. J., and Nickerson, J. E. (1992), Satellite remote sensing of surface energy balance: success, failures and unresolved issues in FIFE. *J. Geophys. Res.* 97:19,061–19,089.

Hipps, L. E., and Kustas, W. P. (1994), Interactions between regional surface fluxes and the atmospheric boundary layer over a heterogeneous watershed. *Water Resour. Res.* 30:1387–1392.

Idso, S. B., Schmugge, T. J., Jackson, R. D., and Reginato, R. J. (1975), The utility of surface temperature measurements for the remote sensing of surface soil water status. *J. Geophys. Res.* 80:3044–3049.

Jackson, R. D. (1982), Soil moisture inferences from thermal-infrared measurements of vegetation temperatures. *IEEE Trans. Geosci. Remote Sens.* GE-20:282–285.

Jackson, R. D., Hatfield, J. L., Reginato, R. J., Idso, S. B., and Pinter, P. J., Jr. (1983), Estimation of daily evapotranspiration from one time-of-day measurements. *Agric. Water Manage.* 7:351–362.

Kanemasu, E. T., Verma, S. B., Smith, S. A., Fritschen, L. J., Wesely, M., Field, R. T., Kustas, W. P., Weaver, H., Stewart, J. B., Gurney, R. J., Panon, G., and Moncrieff, J. B. (1992), Surface flux measurements in FIFE: an overview. *J. Geophys. Res.* 97:18,547–18,555.

Kohsiek, W., De Bruin, H. A. R., The, H., and van den Hurk, B. (1993), Estimation of the sensible heat flux of semi-arid area using surface radiative temperature measurements. *Boundary-Layer Meteorol.* 63:213–230.

Kustas, W. P., Blanford, J. H., Stannard, D. I., Daughtry, C. S. T., Nichols, W. D., and Weltz, M. A. (1994a), Local energy flux estimates for unstable conditions using variance data in semiarid rangelands. *Water Resour. Res.* 30:1241–1259.

Kustas, W. P., Choudhury, B. J., Moran, M. S., Reginato, R. J., Jackson, R. D., Gay, L. W., and Weaver, H. L. (1989), Determination of sensible heat flux over sparse canopy using thermal infrared data. *Agric. For. Meteorol.* 44:197–216.

Kustas, W. P., and Goodrich, D. C. (1994), Preface to Monsoon '90 experiment. *Water Resour. Res.* 30:1211–1225.

Kustas, W. P., Goodrich, D. C., Moran, M. S., et al. (1991), An interdisciplinary field study of the energy and water fluxes in the atmosphere-biosphere system over semiarid rangelands: description and some preliminary results. *Bull. Am. Meteorol. Soc.* 72:1683–1705.

Kustas, W. P., and Norman, J. M. (1996), Use of remote sensing for evapotranspiration monitoring over land surfaces. *Hydrol. Sci. J.* 41:495–516.

Kustas, W. P., Perry, E. M., Doraiswamy, P. C., and Moran, M. S. (1994b), Using satellite remote sensing to extrapolate evapotranspiration estimates in time and space over a semiarid rangeland basin. *Remote Sens. Environ.* 49:275–286.

McNaughton, K. G., and Spriggs, T. W. (1986), A mixed-layer model for regional evaporation. *Boundary-Layer Meteorol.* 34:243–262.

McNaughton, K. G., and Van den Hurk, B. J. J. M. (1995), A "Lagrangian" revision of the resistors in the two-layer model for calculating the energy budget of a plant canopy. *Boundary-Layer Meteorol.* 74:262–288.

Mellor, G. L., and Yamada, T. (1974), A hierarchy of turbulence closure models for planetary boundary layers. *Atmos. Sci.* 31:1791–1806.

Moran, M. S., Clarke, T. R., Kustas, W. P., Weltz, M. A., and Amer, S. A. (1994), Evaluation of hydrologic parameters in semiarid rangeland using remotely sensed spectral data. *Water Resour. Res.* 30:1287–1297.

Nie, D., Kanemasu, E. T., Fritschen, L. J., Weaver, H. L., Smith, E. A., Verma, S. B., Field, R. T., Kustas, W. P., and Stewart, J. B. (1992), An intercomparison of surface energy flux measurement systems used during FIFE 1987. *J. Geophys. Res.* 97:18,715–18,724.

Norman, J. M., Anderson, M. C., and Diak, G. R. (1996), An approach for mapping light-use-efficiency on regional scales using satellite observations. In *Proc. 1996 Int. Geoscience Remote Sensing Symp.*, May 27–31, 1996, 2358–2360, *IEEE*, Seabrook, TX.

Norman, J. M., and Becker, F. (1995), Terminology in thermal infrared remote sensing of natural surfaces. *Remote Sens. Rev.* 12:159–173.

Norman, J. M., and Campbell, G. S. (1983), Application of a plant-environment model to problems in irrigation. In *Advances in Irrigation* (D. I. Hillel, Ed.), Academic Press, New York, pp. 155–188.

Norman, J. M., Chen, J. -L., and Goel, N. S. (1990), Thermal emissivity and infrared temperature dependence of plant canopy architecture and view angle. *Proc. Tenth Annu. Int. Geoscience Remote Sensing Symp.*, Vol. 1, 755–756, *IEEE*, Piscataway, NJ.

Norman, J. M., Divakarla, J., and Goel, N. S. (1995a), Algorithms for extracting information from remote thermal-IR observations of the earth's surface. *Remote Sens. Environ.* 51:157–169.

Norman, J. M., Kustas, W. P., and Humes, K. S. (1995b), A two-source approach for estimating soil and vegetation energy fluxes from observations of directional radiometric surface temperature. *Agric. For. Meteorol.* 77:263–293.

Palluconi, F., Kahle, A. B., Hoover, G., and Conel, J. E. (1990), The spectral emissivity of prairie and pasture grasses at Konza prairie, Kansas. In *Proc. Am. Meteorol. Soc. Symp. on the First ISLSCP Field Experiment (FIFE)*, 77–78, February 7–9, 1990, Anaheim, CA, Am. Meteorol. Soc., Boston, MA.

Price, J. C. (1980), The potential of remotely sensed thermal infrared data to infer surface soil moisture and evaporation. *Water Resour. Res.* 16:787–795.

Price, J. C. (1990), Using spatial context in satellite data to infer regional scale evapotranspiration. *IEEE Trans. Geosci. Remote Sens.* 28:940–948.

Priestley, C. H. B., and Taylor, R. J. (1972), On the assessment of surface heat flux and evaporation using large-scale parameters. *Mon. Weather Rev.* 100:81–92.

Ross, J. (1981), The radiation regime and architecture of plants. In *Task for Vegetation Sciences 3* (H. Lieth, Ed.), Dr. W. Junk, The Hague, Netherlands.

Sauer, T. J., Norman, J. M., Tanner, C. B., and Wilson, T. B. (1995), Measurement of heat and vapor transfer at the soil surface beneath a maize canopy using source plates. *Agric. For. Meteorol.* 75:161–189.

Sellers, P. J., Hall, F. G., Asrar, G., Strebel, D. E., and Murphy, R. E. (1988), The first ISLSCP field experiment (FIFE). *Bull. Am. Meteorol. Soc.* 69:22–27.

Sellers, P. J., Hall, F. G., Asrar, G., Strebel, D. E., and Murphy, R. E. (1992), An overview of the first international satellite land surface climatology project (ISLSCP) field experiment (FIFE). *J. Geophys. Res.* 97:18,345–18,371.

Sellers, P. J., Meeson, B. W., Hall, F. G., Asrar, G., Murphy, R. E., Schiffer, R. A., Bretherton, F. P., Dickinson, R. E., Ellingson, R. G., Field, C. B., Huemmrich, K. F., Justice, C. O., Melack, J. M., Roulet, N. T., Schimel, D. S., and Try, P. D. (1995), Remote sensing of the land surface for studies of global change: models—algorithms—experiments. *Remote Sens. Environ.* 51:1–17.

Sellers, P. J., Tucker, C. J., Collatz, G. J., Los, S. O., Justice, C. O., Dazlich, D. A., and Randall, D. A. (1994), A global 1° by 1° NDVI data set for climate studies, part 2: the generation of global fields of terrestrial biophysical parameters from the NDVI. *Int. J. Remote Sens.* 15:3519–3545.

Shaw, R. H., and Pereira, A. R. (1982), Aerodynamic roughness of a plant canopy: a numerical experiment. *Agric. Meteorol.* 26:51–65.

Smith, E. A., Hsu, A. Y., Crosson, W. L., Field, R. T., Fritschen, L. J., Gurney, R. J., Kanemasu, E. T., Kustas, W. P., Nie, D., Shuttleworth, W. J., Stewart, J. B., Verma, S. B., Weaver, H. L., and Wesely, M. L. (1992), Area-aver-

aged surface fluxes and their time-space variability over the FIFE experimental domain. *J. Geophys. Res.* 97:18,599–18,622.

Stewart, J. B., Kustas, W. P., Humes, K. S., Nichols, W. D., Moran, M. S., and de Bruin, A. A. R. (1994), Sensible heat flux-radiometric surface temperature relationship for eight semiarid areas. *J. Appl. Meteorol.* 33:1110–1117.

Stewart, J. B., Shuttleworth, W. J., Blyth, K., and Lloyd, C. R. (1989), FIFE: a comparison between aerodynamic surface temperature and radiometric surface temperature over sparse prairie grass. *AMS Preprint of the 19th Conf. on Agricultural and Forest Meteorology and 9th Conf. on Biometeorology and Aerobiology*, American Meteorological Society, Charleston, SC, pp. 144–146.

Strebel, D. E., Landis, D. R., Huemmrich, K. F., and Meeson, B. W. (1994), Collected data of the first ISLSCP field experiment. Vol. 1: Surface observations and non-image data sets, published on CD-ROM by NASA.

Sugita, M., Brutsaert, W. (1990), Regional surface fluxes from remotely sensed skin temperature and lower boundary layer measurements. *Water Resour. Res.* 26:2937–2944.

Sugita, M., Brutsaert, W. (1991), Daily evaporation over a region from lower boundary layer profiles measured with radiosondes. *Water Resour. Res.* 27:747–752.

Swiatek, E. (1992), Estimating regional surface fluxes from measured properties of the atmospheric boundary layer in a semiarid ecosystem. M. S. thesis, Utah State Univ., Logan UT.

Taconet, O., Bernard, R., and Vidal-Madjar, D. (1986), Evapotranspiration over an agricultural region using a surface flux/temperature model based on NOAA-AVHRR data. *Clim. Appl. Meteorol.* 25:285–307.

Tennekes, H. (1973), A model for the dynamics of the inversion above a convective boundary layer. *J. Atmos. Sci.* 30:558–567.

Tillman, J. E. (1972), The indirect determination of stability, heat and momentum fluxes in the atmospheric boundary layer from simple scalar variables during dry conditions. *J. Appl. Meteorol.* 11:783–792.

Vining, R. C., and Blad, B. L. (1992), Estimation of sensible heat flux from remotely sensed canopy temperatures. *J. Geophys. Res.* 97:18,951–18,954.

Wetzel, P. J., Atlas, D., and Woodward, R. (1984), Determining soil moisture from geosynchronous satellite infrared data: a feasibility study. *J. Clim. Appl. Meteorol.* 23:375–391.

Wilmott, C. J. (1981), On the validation of models. *Phys. Geogr.* 2:184–194.

Willmott, C. J. (1982), Some comments on the evaluation of model performance. *Bull. Am. Meteorol. Soc.* 63:1309–1313.

Zhan, X., Kustas, W. P., and Humes, K. S. (1996), An intercomparison study on models of sensible heat flux over partial canopy surfaces with remotely sensed surface temperature. *Remote Sens. Environ.* 58:242–256.